Geochimica et Cosmochimica Acta
July 2011, Volume 75, Issue 14, Pages 4037-4052
http://dx.doi.org/10.1016/j.gca.2011.05.001

Mercury in the Southern Ocean

Daniel Cossa[a, *], Lars-Eric Heimbürger[a], Delphine Lannuzel[b, c], Stephen R. Rintoul[b, d, e], Edward C.V. Butler[b, d, e], Andrew R. Bowie[b], Bernard Averty[f], Roslyn J. Watson[d] and Tomas Remenyi[b]

[a] Ifremer, Centre for the Mediterranean Sea, BP 330, F.83507 La Seyne sur Mer, France
[b] Antarctic Climate and Ecosystems Cooperative Research Centre (ACE CRC), Hobart, Tasmania 7001, Australia
[c] Institute for Marine and Antarctic Studies, Hobart, Tasmania 7001, Australia
[d] Centre for Australian Weather and Climate Research (CAWCR), Hobart, Tasmania 7000, Australia
[e] Wealth from Oceans National Research Flagship, CSIRO Marine and Atmospheric Research, Hobart, Tasmania 7001, Australia
[f] Ifremer, Nantes Centre, BP 21105, F.44311 Nantes Cedex 03, France

*: Corresponding author : Daniel Cossa, email address : dcossa@ifremer.fr

Abstract:

We present here the first mercury speciation study in the water column of the Southern Ocean, using a high-resolution south-to-north section (27 stations from 65.50°S to 44.00°S) with up to 15 depths (0–4440 m) between Antarctica and Tasmania (Australia) along the 140°E meridian. In addition, in order to explore the role of sea ice in Hg cycling, a study of mercury speciation in the "snow–sea ice–seawater" continuum was conducted at a coastal site, near the Australian Casey station (66.40°S; 101.14°E). In the open ocean waters, total Hg (Hg_T) concentrations varied from 0.63 to 2.76 pmol L^{-1} with "transient-type" vertical profiles and a latitudinal distribution suggesting an atmospheric mercury source south of the Southern Polar Front (SPF) and a surface removal north of the Subantartic Front (SAF). Slightly higher mean Hg_T concentrations (1.35 ± 0.39 pmol L^{-1}) were measured in Antarctic Bottom Water (AABW) compared to Antarctic Intermediate water (AAIW) (1.15 ± 0.22 pmol L^{-1}). Labile Hg (Hg_R) concentrations varied from 0.01 to 2.28 pmol L^{-1}, with a distribution showing that the Hg_T enrichment south of the SPF consisted mainly of Hg_R (67 ± 23%), whereas, in contrast, the percentage was half that in surface waters north of PFZ (33 ± 23%). Methylated mercury species ($MeHg_T$) concentrations ranged from 0.02 to 0.86 pmol L^{-1}. All vertical $MeHg_T$ profiles exhibited roughly the same pattern, with low concentrations observed in the surface layer and increasing concentrations with depth up to an intermediate depth maximum. As for Hg_T, low mean $MeHg_T$ concentrations were associated with AAIW, and higher ones with AABW. The maximum of $MeHg_T$ concentration at each station was systematically observed within the oxygen minimum zone, with a statistically significant $MeHg_T$ *vs* Apparent Oxygen Utilization (AOU) relationship ($p < 0.001$). The proportion of Hg_T as methylated species was lower than 5% in the surface waters, around 50% in deep waters below 1000 m, reaching a maximum of 78% south of the SPF. At Casey coastal station Hg_T and Hg_R concentrations found in the "snow–sea ice–seawater" continuum were one order of magnitude higher than those measured in open ocean waters. The distribution of Hg_T there suggests an atmospheric Hg deposition with snow and a fractionation process during sea ice formation, which excludes Hg from the ice with a parallel Hg enrichment of brine, probably concurring with the Hg enrichment of AABW observed in the open ocean waters. Contrastingly, $MeHg_T$ concentrations in the sea ice environment were in the same range as in the open ocean waters, remaining below 0.45 pmol L^{-1}. The $MeHg_T$ vertical profile through the continuum suggests different sources, including atmosphere, seawater and methylation in basal ice. Whereas Hg_T concentrations in the water samples

collected between the Antarctic continent and Tasmania are comparable to recent measurements made in the other parts of the World Ocean (e.g., Soerensen et al., 2010), the Hg species distribution suggests distinct features in the Southern Ocean Hg cycle: (i) a net atmospheric Hg deposition on surface water near the ice edge, (ii) the Hg enrichment in brine during sea ice formation, and (iii) a net methylation of Hg south of the SPF.

Keywords : mercury, methyl mercury, water column, sea ice, Southern Ocean, Antarctica

Introduction

Mercury is widely distributed in the oceans as a result of long-54 range atmospheric transport and deposition by wet and dry processes. The stability of its neutral and volatile species (mainly elemental (Hg0) and dimethylmercury (DMHg)) and the reactivity of its charged species (mainly chlorocomplexes) causes it to be intensively recycled between the lower troposphere and the ocean surface, and actively scavenged by particula matter (e.g., Mason and Gill, 2005). All chemical forms are intricately linked together through the divalent pool (HgII), by various chemical reactions and microbiological transformations, such as methylation/demethylation and oxidation/reduction reactions (see reviews by Mason and Gill, 2005 and Fitzgerald et al., 2007). Methylation/demethylation reactions control the abundance of monomethylmercury (MMHg) in seawater, a neuro-toxic species that is biomagnified in the food web, posing health s for consumers of marine seafood. Oxidation/reduction reactions influence the transfer of mercury between surface water and the troposphere. Many of these reactions involve phase changes, which, combined with spatial variations in ocean circulation, t intensity of the biological pump and the deposition of Hg, can generate large spatial heterogeneity in the distribution of the various Hg species.

Because of the analytical challenges of measuring Hg species concentrations in oceanic waters, the distribution of Hg species in the main oceanic water masses is still poorly documented (see reviews by Fitzgerald and Lamborg, 2003; Mason and Gill, 2005; Fitzgerald et al., 2007; Sunderland and Mason, 2007). The Atlantic and North Pacific oceans, and the Mediterranean Sea are the most investigated regions (Mason and Fitzgerald, 1990, 1992 and 1993; Cossa et al., 1997, 2009; Mason and et al., 1998, and 2001; Mason and Sullivan 1999; Horvat el al., 2003, Kotnick et al., 2007; Laurier et al., 2004; Cossa and Coquery, 2005; Heimbürger et al., 2010), but few measurements have been made in other major open ocean regions, such as the Indian, the South Pacific, the Central Arctic, and the Southern Oceans. One exception is a study by Pongratz and Heumann (1998) who reported MMHg and DMHg concentrations in surface and subsurface sea-water samples from the English Channel in the North At ic (51°N) to pack-ice border of Antarctica (58°S). Furthermore, due to the lack of precision of measurements at the subpicomolar level, the observed distributions have failed, until n to reveal systematic horizontal geographical trends consistent with the oceanic circulation and biological characteristics, with the

sole exception being the observation of higher Hg concentrations in Atlantic surface waters compared to those found in the Pacific (Mason and Gill, 2005). Conversely, systematic vertical trends have been shown, with Hg_T profiles typical of "particle reactive" or "transient" trace elements, such as Pb, implying a short residence time the ocean (Bruland and Lohan, 2003; Fitzgerald et al., 2007). This is the case for Pacific Ocean and Mediterranean Sea Hg_T distributions in the water column, with elevated concentrations in surface water consistent with an atmospheric Hg source (Laurier et al., 2004; Cossa Coquery, 2005). While the Hg_T pattern describes the overall behavior of Hg, the vertical distributions of particular chemical species reveal contrasting behaviors. Both MMHg and DMHg are present in very low concentrations in surface water, due to the instability of these molecules in light (Bergquist and Blum, 2007), and increase with depth, peaking in the low oxygen region, where net Hg methylation by microbial activity, driven by the decomposition of the sinking P , is assumed to take place (Mason and Fitzgerald, 1990; Cossa et al., 2009; Sunderland et al., 2009; Heimbürger et al., 2010). Hg^0 is found both at the surface, as the result of photochemically and biologically mediated reduction of Hg^{II}, and at depth as the end product of the decomposition of methylated species (Mason and Fitzgerald, 1993; Mason and Gill, 2005).

Polar zones exhibit unique characteristics, chiefly in temperature and light, which make its Hg cycle unique. The main particularity consists of the rapid oxidation of atmospheric Hg^0 as hygroscopic Hg^{II} (RGHg for reactive gaseous mercury) in the polar spri e, by sea-salt-derived bromine released into the atmosphere during sea ice formation (Schroeder et al., 1998; Lindberg et al., 2001; Ariya et al., 2002). RGHg is deposited onto snow surfaces with a potential transfer to the ocean upon thawing (Lindberg et al., 2 ; Brooks et al., 2008). This phenomenon, called an Hg depletion event (MDE), was first discovered in the Arctic (Schroeder et al., 1998), then observed in coastal Antarctica (Ebinghaus et al., 2002; Sproveri et al., 2002; Bargalgi et al., 2005). However, while the Hg cycle in the Arctic has been extensively documented, only a few attempts have been made to study the Hg cycle in the Southern Polar region. Gaseous elemental mercury (Hg^0), which is transported on a hemispheric scale (Slerm et al., 1995), is present in slightly higher concentrations (7.7 ± 1.9 pmol m^{-3}) in the coastal Antarctic marine boundary layer (MBL) compared to more northern sts (e.g., the mean for New Zealand is 5.9 ± 0.8 pmol m^{-3}) (Soerensen et al., 2010). Furthermore, the same authors state that the Antarctic environment exhibits elevated RGHg concentrations (0.21 ± 0.19 pmol m^{-3}) which are

more than 10-fold the concentrations detected further north. According to a recent review by Dommergue et al. (2010), atmospheric Hg and ozone depletion events are detectable along the Antarctic sea ice edge, in polynyas, and between pack ice and fast ice, with oxidatio of Hg^0 probably more intense than in the Arctic, perhaps due the nearly constant oxidized Hg enhancement over the sunlit period on the Antarctic co ent. While reductive re-emission of Hg to the trophosphere remains to be assessed, Dommergue et al. 10) concluded that the fast reactivity of Hg^0 and the presence of Hg^{II} from late winter to summer may result in an important net input of atmospheric Hg onto Antarctic surfaces. T very high RGHg concentrations (0.2 – 5.0 pmol m^{-3}) (Sproveri et al., 2002; Temme et al., 2003; Soerense et al., 2010) are likely to result in Hg deposition onto coastal snow packs leading to elevated Hg_T concentrations (up to 2140 pmol L^{-1}) in the surface snow at the fast-ice edge adjacent to the freezing ocean (Brooks et al., 2008). The same authors suggest Hg is transferred to the surface seawater in summer during thawing. In addition, high Hg concentrations (mainly as methylmercury) have been observed in Antarctica biota, despite the long distance from anthropogenic sources (Bargagli, 2008; Bargalgi et al., 2005). Albatross and petrels in the Southern O (SO) have the largest total and methylmercury concentrations yet recorded in seabirds to 680 µg g^{-1}, wet weight according to Hindell et al., 1999). This huge bioaccumulation is rather surprising for a supposedly pristine environment, and the origin of methylmercury, the biomagnified Hg species in marine organisms, in the SO remains unknown.

The lack of Hg observations in the Antarctic environment has prevented identification of the factors controlling the distribution and speciation of mercury in the SO, including the high Hg bioaccumulation in open-ocean and coastal ecosystems. Here, we present the first Hg measurements (including total mercury and labile, dissolved gaseous and methylated species) in the water column of the SO, using a high-resolution south-to-north section (27 stations from 65.5°S to 44°S) with up to 15 depths (0-4440 m) between Antarctica and Tasmania (Australia) along the 140°E meridian (Fig. 1).

In addition, in order to explore the role of the sea i in the Hg cycling, a special study was devoted to Hg speciation in the "snow-ice-brine-seawater" continuum at a coastal site, near the Australian Casey station. More specifically, we wanted to address the following questions: (i) what are the level and general distribution of Hg_T concentrations in the waters of the SO, and is there any indication for sources and sinks? (ii) What re the characteristics of the Hg speciation

in the waters, which may shed light on Hg cycling specificity of the SO? (iii) What is the role of the sea ice (formation and melting) in the Hg_T distribution, speciation and cycling in the SO? And finally (iv) how do our findings contribute to explaining the Hg hyperbioaccumulation in Antarctic food webs?

2. SITE

2.1. The Southern ocean SR3 CASO-GEOTRACES transect

The SR3 CASO-GEOTRACES transect took place between 22 March and 17 April 2008. From south to north, the SR3 section crosses the Southern Antarctic Circumpolar Current Front (SACCF), the Polar Front (SPF), the Subantarctic Front (SAF) and the Subtropical Front (STF) (Orsi et al., 1995; Sokolov and Rintoul, 2002, 2007). ese fronts mark sharp horizontal gradients in water mass properties. Between the fronts lie zones with sim water mass characteristics: the Subtropical Zone (STZ), the Subantarctic Zone (SAZ), the Polar Frontal Zone (PFZ), the Antarctic Zone (AZ), and the Southern Zone Z), between the SACCF and the Antarctic continent.

The relatively saline Circumpolar Deep Water (CDW) occupies the largest volume of the Southern Ocean (SO) and lies between the fresher Antarctic Intermediate Water (AAIW) above and fresher Antarctic Bottom Water (AABW) below (Rintoul and Bullister, 1999). The source of CDW is the North Atlantic Deep Water (NADW) exported from the Atlantic Ocean. The CDW is often divided into the Lower CDW (LCDW), corresponding to a deep salinity maximum layer, and the slightly less dense Upper CDW (UCDW), which is defined by an oxygen minimum layer (Rintoul, 2006). The low oxygen of the UCDW is the result of bacterial decomposition of organic matter occurring during the transit of the CDW through the deep layers of the Indian and Pacific basins. The oxygen-poor and nutrient-rich UCDW shoals from north to south across the SO and approaches the surface near the SACCF where it supports high primary production in the AZ and the SZ. Primary productivity in this region is further enhanced by melting sea ice in spring and summer, which both enhances light levels by stabilizing the water column and supplies micro-nutrients, such as iron (Sullivan et al., 1993; Sedwick and Di Tullio, 1997; Lannuzel et al., 2008). Nutrient concentrations and primary production are generally lower in the SAZ and PFZ. The

poleward flow and upwelling of the UCDW is balanced by sinking and the equatorward flow of Antarctic Intermediate Water (AAIW) and Antarctic Bottom Water (AABW).

2.1. The Casey coastal station

The fast ice study took place in November 2009 in first year sea ice adjacent t "Jack's Donga" hut approximately 12 km northeast of the Casey Station (Australian East Antarctic sector) (66° 13.11'S; 110° 39.03'E). Our sampling site was located 500 m off the coast and encircled by islands from the Swain group. Adelie penguin colonies, icebergs, exposed rock moraine and glacial ice surrounded our sampling area. The fast ice was 120 cm thick, undeformed (i.e., sea ice grew under thermodynamic processes – no rafting involved), level and sitting only 15 to 17 m above the seafloor.

3. MATERIAL AND METHODS

3.1. Southern ocean sampling

Sampling stations are given in figure 1, and the coordinates, dates of sampling and ottom depths are given in a supplementary table (Web appendix 1). All sampling methods followed recommended GEOTRACES (www.geotraces.org) protocols as closely as possible. The water column was sampled on the IPY- GEOTRACES section (from Antarctica to Tasmania, Fig. 1) along the CASO 140°E SR3 meridian during voyage V6 of R/V AURORA AUSTRALIS. Water-column-profile samples were collected using externally closing, Teflon-lined Niskin-1010X® samplers, upon which all remaining metal parts have been replaced by e-metal-clean equivalents, deployed on an autonomous 1018 intelligent rosette system specially developed for trace metal work (General Oceanics Inc., USA) (Bowie et al., 2009). Twenty-seven (27) stations were occupied from 66°S to 44°S, with between 7 and 15 samples collected from the surface down to 4440 m depth, yielding a total of 241 water sa les. Reactive mercury (Hg_R, see section 3.3. below for definition) and dissolved gaseous mercu (DGHg) sub-samples (201 and 59 respectively) were analyzed on board. Sub-samples for total (Hg_T) and total methylated mercury species ($MeHg_T$, see section 3.3. below for definition) measurements (71 and 241 respectively) were immediately withdrawn into acid-cleaned Teflon® (FEP) bottles, following ultraclean sample handling protocols within an ISO class-5 clean air laboratory container. Samples were

acidified with HCl (0.4%, v/v, Suprapur®, Merck), hermetically sealed, double-wrapped in polyethylene bags, and kept in the dark at +4°C until analysis in the home laboratory.

3.2. Casey station sampling

All sample preparation and collection techniques were nducted according to Lannuzel et al. (2006). Snow was first collected upwind using acid-cleaned plastic shovels and transferred into polyethylene (PE) containers. Ice cores were then collected using a custom-made corer (Lichtert Industrie, Belgium) designed and tested for ace metal sampling. One top (0-6 cm), two intermediate (30-36 cm and 70-76 cm) and two bottom (lowermost 12 cm) ice sections were collected from the same site every 3 days from the 11th until the 20th of November. Ice sections were then placed into individual acid-cleaned PE containers and transported to the station laboratory, where they were melted in the dark at ambient temperature before being processed. Brines were drained from "sack holes" drilled at 50 cm and 100 cm deep in the ice cover. The liquid brine was collected using a peristaltic pump (M sterflex®, Cole Parmer) coupled with acid cleaned C-Flex tubing. Seawater was collected using a 7 L polycarbonate (PC) Helmond-Byrne (H-B) sampler attached to a Kevlar® line (Sedwick et al., 1997). The H-B sampler was lowered through the ice cover and triggered at 0, 5 and 10 m depths using an all-Teflon messenger. The collected seawater was decanted into 1 L acid-washed Low Density Polyethylene (LDPE) Nalgene® bottles, double-bagged and taken back to the Casey station laboratory. Standard trace metal techniques were followed with all laboratory-based processing taking place under a class-100 laminar flow hood. Melted sea ice, snow, sack-hole brine and seawater samples were filtered through acid washed 0.2 µm PC membrane filters (47-mm diameter, Sterlitech®) and using Sartorius® filtration devices coupled with a vacuum pump (Nalgene®). Filtered volumes ranged between 100 and 1000 mL depending on the type of sample. A 125-mL aliquot from the <0.2-µm fraction was collected in acid-cleaned Teflon® (FEP) bottles, acidified with 50 µL HCl (0.4% v/v Seastar Baseline®, Choice Analytical) sealed, double-bagged, and stored in the dark at 4°C until analysis in the home laboratory.

3.3. Analyses

All Hg determinations were made using atomic fluorescence spectroscopy (AFS, Tekran, model 2500®).

Easily reducible mercury (labile), so-called “reactive” mercury (Hg_R), was determined on board immediately after sampling in unamended seawater (50-100 mL). The method consisted of a direct reduction of Hg_R by an acidic stannous chloride solution (0.002 mol L^{-1}), the amalgamation of elemental Hg on a gold trap, and its subsequent qua cation by AFS. Since the samples were not bubbled before analysis, this Hg fraction is assumed to represent Hg^0 and Hg ions associated with inorganic or very weak organic complexing agents (Lamborg et al., 2003).

Total mercury (Hg_T) was determined, within 3 months after sampling, on a ified (HCl, 0.4% v/v Suprapur®, Merck) samples, stored in FEP Teflon bottles. The method con d of an oxidation of the sample with an acidic BrCl solution (20 µmol.L^{-1}), followed by a reduction of the oxidized Hg by an acidic stannous chloride solution (0.002 mol.L^{-1}), the amalgamation of the reduced Hg on a gold trap and its subsequent quantification by AFS. This method is known as the US-EPA method N° 1631.

Accuracy for Hg_R and Hg_T was checked using the CRM ORMS-3 of the National Research Council of Canada and BCR-579 of the Institute for Reference Materials and Measurements for Europe. For means (± 95% confidence limits), we found 3.9 ± 4.5 pmol.L^{-1} (certified value: 62.8 ± 5.5 pmol.L^{-1}) for ORMS-3 and 1.9 ± 0.2 pmol.L^{-1} for BCR-579 (certified value: 1.9 ± 0.5 pmol L^{-1}). The detection limit, 3 times the standard deviation of 5 blank replicates, was 0.15 pmol.L^{-1}. The analytical reproducibility (5 replicate analyses of the BCR-579) was better than 10 %. The reproducibility estimated on a CRM is assumed to be va for the analyzed seawater samples. The possible drift in accuracy during analyses was checked by inserting a CRM every tenth measurement.

Dissolved gaseous mercury (DGHg) was also determined on board. The method consisted of a direct bubbling of a 1 L unamended sample, the amalgamation of elemental Hg on a gold trap and its subsequent quantification by AFS. This Hg fraction is umed to represent both dissolved elemental Hg and the volatile dimethylmercury (DGHg=Hg^0+DMHg). The AFS calibration for DGHg measurements consisted of injections, every tenth sample, of saturated Hg vapor at known temperatures through a septum located before the amalgamation trap. The detection limit (3 times the standard deviation of 5 blank replicates) was 0.05 pmol.L^{-1}. Within the range of concentrations measured, the analytical reproducibility was approximately 12 %.

We measured monomethylmercury (MMHg) using hydride generation, purge and cryo-trapping gas chromatography, and the detection as elemental Hg r by AFS. However, under acidic sample storage conditions (0.4% HCl, v/v), the measured MMHg accounts for both methylated species ($MeHg_T$=MMHg+DMHg). Indeed, MMHg is stable in acidified seawater for at least 250 days, whereas DMHg rapidly decomposes under similar conditions (Parker and Bloom, 2005). The quantitative conversion of DMHg into MMHg in acidified seawater has recently been confirmed (Black et al., 2009). The analytical protocol was designed by Stoichev et al. (2004) and detailed by Cossa et al. (2009). The hydrides are ormed within a glass reactor, and the column used is a glass tube filled with Chromosorb W/AW-DMCS® impregnated with 15% OV-3®. Within the range of concentrations measured, the analytical reproducibility was approximately 15%. The detection limit, 3 times the standard deviation of 5 blank replicates, was 0.015 $pmol.L^{-1}$. Accuracy was checked using the certified reference material (CRM) ERM-AE670 ($CH_3\ ^{202}HgCl$ in 2% v/v ethanol/water, IRMM, European Commission). The $MeHg_T$ measurements were performed within 2 months after sampling.

Dissolved oxygen was measured by Sea-Bird SBE 43® polarographic-type sensor mounted on a CTD rosette incorporating Sea-Bird 9*plus*® underwater unit. Each profile was recalibrated with data obtained from discrete seawater samples, titrated using a variation of the standard Winkler method with an automatic titration system (Cowley, 1999), based on the method of Knapp et al. (1990). Soluble reactive phosphorus (SRP) concentrations ere determined (along with nitrate-plus-nitrite and reactive silicon) using an automated colorimetric analyser (Lachat QuikChem 8000). For SRP, it is a modification of the standard m bdenum-blue method (Grasshoff, 1976; Cowley 1999).

4. RESULTS

4.1. Hydrology, oxygen and nutrients

The salinity, temperature, dissolved oxygen and nutrie distributions (Fig. 2) follow the typical patterns found along the SR3 transect (Rintoul and Bullister, 1999). The SAF was located between 51.0°S to 52.7°S, and SACCF, associated with the upwelling of the Antarctica divergence, at 63.4°S, and the northern ice pack limit was found in the SZ at 64°4'S (Fig. 2). Chlorophyll *a* distributions in the upper 200 m along the SR3 transect increased from south to

north, with very little biomass noted south of ~57°S (Chl*a* < ~0.2 µg.L^{-1}). A deep Chl*a* maximum was noted around 110 m in polar waters at 56°S, with higher plant biomass in the SAZ, and significantly larger Chl*a* concentrations (> 0.7 µg.L^{-1}) were observed in subtropical waters north of 46°S close to Tasmania. It was likely that biologic uptake along the SR3 transect earlier in the season (spring-summer) resulted in widespread iron limitation during r period of sampling (fall).

4.2. Hg_T distribution in the SO

Measured Hg_T concentrations varied from 0.63 to 2.76 pmol.L^{-1}, with an arithmetical mean of 1.33 pmol.L^{-1}, a standard deviation of 0.45 pmol.L^{-}1 and a median of 1.20 pmol.L^{-1} for the 71 samples analyzed. Seventy-five percent of the values were found between 0.86 and 1.44 pmol L^{-1}. According to our speciation measurements, in deep waters (>200 m) 79 ± 20 % of Hg_T consisted of easily reducible mercury and methylated species, whereas the same species accounted for only 37 ± 30 % in the upper layer (<200 m). According to the known Hg species present in seawater (Mason and Gill, 2005), the unaccounted for Hg likely consisted of unmethylated organic and "unreactive" inorganic Hg^{II} compounds. The former are expected to occur in the biologically productive zone (<200 m), where organic matter is relatively abundant, the latter deeper in the water column.

The main variations occurred within the upper 200 m and near the bottom (Fig. 3). This type of vertical distribution is similar to observations in other oceanic regions (Mason and Sullivan, 1999; Laurier et al., 2004; Cossa and Coquery, 2005) and is consistent with the idea that Hg_T distribution is governed by (i) active air-sea exchange which affects Hg^0 concentrations in the mixed layer, and (ii) the affinity of various species of Hg^{II} for both planktonic and inorganic particulate matter ($\log K_D$~5). Generally, these Hg_T profiles illustrate a "transient-type" distribution (Fitzgerald et al., 2007), with atmospherically enhanced Hg levels at the surface and scavenging in the upper ocean. Surface Hg concentrations are comparable with those from the South Atlantic (Mason and Sullivan, 1999), and from the Pacific Ocean (Mason and Fitzgerald, 1993; Laurier et al., 1993), which are = 2 pmol.L^{-1}. Highest surface Hg_T concentrations were found at stations N-02, N-03, and N-08 south of the SPF and the lowest north of the PFZ (F 3). This distribution suggests an Hg net deposition south f the SPF and a net surface removal north of the SAF. In deeper layers, Hg concentrations are relatively constant and consistent with observations in the Pacific Ocean and the Mediterranean Sea (Laurier et al., 2004; Cossa and

Coquery, 2005). In order to examine possible Hg_T differences linked to a water mass source, we characterized the different water masses found along the transect, based on depth, salinity and temperature (Table 1). We observed slightly different an Hg_T concentrations: 1.35, 1.19 and 1.15 pmol.L^{-1}, for AABW, CDW, and AAIW, respectively (Table 1). Noteworthy is the facr that the highest mean concentration was found in AABW, with a small difference between AABW and AAIW ($p<0.15$ for *t*-tests, Table 2). The AAIW mean concentration calculated here is consistent with a measurement made by Mason and Sullivan (1999) in AAIW samples identified much farther north (17°S; 25°W) based on values plotte as 0.9 ± 0.1 pmol.L^{-1} in the salinity minimum (Figure 8 of their paper).

4.3. Hg_R distribution in the SO

Hg_R concentrations varied from 0.01 to 2.28 pmol.L^{-1}, with an arithmetic mean of 0.34 pmol.L^{-1}, a standard deviation of 0.35 pmol.L^{-1}and a median of 0.33 pmol.L^{-1} for the 201 samples analyzed. As for Hg_T, the main variations of Hg_R concentrations occurred within the upper 200 m (Fig. 4) with low concentrations (< 0.2 pmol.L^{-1}) north of the SAF (Stns. N-13 to N-27) and the highest values (> 0.5 pmol.L^{-1}) south of the SPF (Stns. N-01 to N-08), notably in the SZ (Fig. 4). This distribution shows that the southerly Hg_T enrichment (Fig. 3) was mainly present as Hg_R (67 ± 23%), whereas, Hg_R accounted for only half as much (33 ± 23%) in surface waters north of SAF (Stns. N-17 to N-27). Intermediate and deep Hg_R concentrations converged to values around 0.45 ± 0.10 pmol.L^{-1} without any notable spatial trends. Mean Hg_R concentrations calculated for the main water masses showed small differences between BW, AAIW and CDW (Table 2).

4.4. $MeHg_T$ distribution in the SO

$MeHg_T$ concentrations ranged between 0.02 to 0.86 pmol.L^{-1} with an arithmetic mean of 0.29 pmol.L^{-1}, a standard deviation of 0.21 pmol.L^{-1} and a median of 0.23 pmol.L^{-1} for the 241 samples analyzed. All vertical $MeHg_T$ profiles exhibited roughly the same pattern with low concentrations in the surface mixed layer (0-100 m) (except at three stations N-03, N-09 and N-18, where surface maxima were observed), and increasing concentrations with depth to an intermediate maximum. Deeper in the water column, $MeHg_T$ concentrations decreased or remained relatively constant (Fig. 5a). Lowest values 2 pmol.L^{-1}) were observed within the upper 100 m of the PFZ (Stns. N-07, 08, 11, 12, 13 and 15) (Fig. 6). Low mean $MeHg_T$ concentrations were also associated with AAIW, which d red significantly from AABW

($p<0.05$, Table 2). Maximum $MeHg_T$ concentrations at each station were systematically observed within the oxygen minimum zone (the $MeHg_T$ *vs* AOU relationship is statistically significant with $p<0.001$, $R^2=0.722$, n=236) as usually found in the oceanic water c ns (Mason and Fitzgerald, 1990, Cossa et al., 1997, 2009; Sunderland et al., 2009; Heimbürger et al., 2010). The $MeHg_T$ maximum followed the upper part of CDW as it shoaled m 2000 m in the STZ and SAZ to outcrop at the sea surface in the AZ (Fig. 6), here the highest values were observed (0.81 and 0.86 pmol.L^{-1} at Stns. N-05 and N-08, respectively) (Fig. 5b). The proportion of Hg_T as methylated species was lower than 5% in the surface waters, around 50% in deep waters below 1000m, peaking up to 78% in the low oxygen waters south of the SPF (Figs. 2c and 5c). These proportions in intermediate and deep waters are relatively elevated compared to proportions compiled from different parts of the World Ocean, which vary from a few percent in the North Atlantic up to 35% in the Mediterranean (see Table 10-1 in Mason and Gill, 2005). Note that the $MeHg_T$ concentrations remain relatively high in deep waters, suggesting a high stability of methylated Hg when these molecules are out of the influence of light.

4.5. DGHg distribution in the SO

DGHg concentrations ranged between <0.01 to 0.59 pmol.L^{-1} with an arithmetic mean of 0.19 pmol.L^{-1}, a standard deviation of 0.11pmol L^{-1} and a median of 0.21 pmol.L^{-1} for the 58 samples analyzed. The vertical DGHg distributions exhibited a pattern with larger variations in the upper 200 m (from <0.01 to 0.59 pmol.L^{-1}), and more homogeneous concentrations at depth (0.20 – 0.31 pmol.L^{-1}) (Fig. 7). Highest DGHg concentrations were measured etween 100 and 200 m at stations south of the SPF (Stns. N-04 and N-07, Fig. 7). According to the $MeHg_T$ profiles (Fig. 5a) it is unlikely that this DGHg consists of DMHg; more probably DGHg is mostly present as Hg^0, the end-product of demethylation. The depth of the mixed layer at these two stations is 100 m, suggesting an intense outgassing of Hg^0 from the well-mixed layer to the atmosphere and its accumulation below. At lower latitudes (Stns. N-17, N-20 and N-23), very low DGHg concentrations were observed in the top 200 m as observed for Hg_R,. While part of the DGHg may be made up of DMHg in intermediate and deep waters (Mason and Gill, 2005), DGHg constituted a high proportion of Hg_R (up to 90%) between 0 and 200 m, where DMHg is supposed to be absent or negligible. The DGHg mean concentrations did not differ significantly with water masses (Tables 1 and 2).

4.6. Mercury speciation in coastal sea ice

The most striking feature of the Hg_T data collected at the shallow coastal station near Casey (seafloor < 20 m deep) is that the Hg_T concentrations, ranging from 0.9 to 27.8 pmol.L^{-1}, were one order of magnitude higher than those measured in open sea waters. Figure 8 illustrates the distribution of Hg_T found in the snow and sea ice (Fig. 8a-e) and in seawater below the ice (Fig. 8f-j). Detailed data, with sack-hole brine values, are given as supplementary information in the Web appendix 2. High Hg_T concentrations occurred in snow, sack-hole brine and seawater, compared to bulk sea ice (Web appendix 2). Hg_T distributions in sea ice were generally 'C'-shaped, with higher concentrations in the top and bott parts of the sea ice cover (Fig. 8). The 'C'-shape profile has been described in the case of sea ice bulk salinity in many other field studies (e.g. Nakawo and Sinha, 1981; Weeks and Ackley, 1986; Eicken, 1992) as a result of the combined effects of initial salt entrapment, brine drainage and brine expulsion. Such tributions have also been previously reported for other trace metals in Antarctic pack ice (Lannuzel et al., 2010). Variability between sampling days (Fig. 8) may, however, simply reflect the spatial heterogeneity of the area (ice cores were separated by up to 10 m on different sampling days). The overall Hg_R distribution (Web appendix 2) follows the same patter as Hg_T, with variable proportion 10 to 100% of the Hg_T as Hg_R. Highest Hg_R/Hg_T ratios were often found within snow and brine (except on the 17 November samples, Web appendix 2). In contrast to Hg_T and Hg_R, $MeHg_T$ concentrations were in the range of those encountered in open ocean waters, remaining below 0.45 pmol.L^{-1}. The $MeHg_T$ vertical profile through the "snow-sea ice-seawater" continuum was complex (Fig. 8). A peak concentration was observed at the base of the sea ice, where high organic matter concentration and autotrophic activity present (Web appendix 2; Fig. 8). In snow samples relatively high $MeHg_T$ levels were found (0.34 pmol L^{-1}). This complex structure suggests different sources of methylmercury, including atmosphere, marine water and *in situ* methylation. The results of a Principal Component Analysis performed on salinity, particulate organic carbon (POC), Chl*a*, Hg_T, Hg_R and $MeHg_T$ in the sea ice brine and seawater indicate that 74% of the whole variability of these parameters is explained by two factors and that Hg_T and Hg_R covaried with salinity, whereas $MeHg_T$ covaried with POC and Chl*a* (Web appendix 3). This supports the ideas that in sea ice environment the ino nic Hg distribution is governed by sea salt exclusion and methylated mercury distribution is erned by biological processes.

5. DISCUSSION

The chemistry of Hg in ocean water is more complex than that of any other trace elements. Many chemical reactions occur between the deposition of atmospheric Hg on the ocean surface and the burial of Hg in the sediment and/or bioaccumulation in the food chain. In the dissolved phase Hg may exist as Hg^0 or, Hg^{II} bound to inorganic (mainly chloride or sulfide) or organic ligands (mainly methyl or thiol groups) (Mason and Gill, 2005). Methylated Hg species ($MeHg_T$) comprise neutral DMHg and $MMHg^+$ bound chiefly to chloride, sulfide or thiol. Mercury speciation performed on board and in the labor y, allowed us to differentiate operationally defined species, namely DGHg, which includes Hg^0 and DMHg, $MeHg_T$ which includes MMHg and DMHg, and the labile Hg, so-called reactive mercury (Hg_R), which is assumed to represent both Hg^0 and Hg^{II}, associated with inorganic or very weak organic complexing agents (Lamborg et al., 2003). Mercury transformations known to occur in the oceanic waters and at the MBL include (i) redox reactions between Hg^{II} and Hg^0, (ii) methylation-demethylation, and (iii) heterogeneous reactions, such as the sorption of charged species and the solid solution of neutral species. All these chemical forms are intricately linked togeth through the divalent pool (Hg^{II}) and are often catalyzed by biological activity, especially Hg ethylation (Mason and Gill, 2005; Heimbürger et al., 2010). A schematic view of the ocea Hg cycle can be summarized as follows. Elemental mercury is oxidized at the MBL and deposited onto the sea surface *via* dry or wet processes. These Hg^{II} species are either reduced again (and re-emitted in the troposphere), or bound to mineral or organic ligands, and/or sorbed onto phytoplankton within the photic zone. Inorganic Hg transported downward attached to particles (mainly biogenic), can be biomethylated in the water column with rates depending on the type of microbial ecosystem associated with phytoplankton degradation (Heimbürger al., 2010). Conversely, biological and photochemical demethylations (with Hg^0 as an end product) occurs concurrently, so that methylmercury concentrations reflect the net effect of methylation-demethylation. Although Hg sinking with large particles to the sediment may be in ved in early diagenetic transformations that take place at the ocean-sediment interface of the abyssal sediments (Gobeil et al., 1999), these sediments constitute the final sink for Hg in the open ocean environment.

5.1. Role of sea ice in the distribution of Hg in seaw r

According to a study in a coastal region of Antarctica (McMurdo/Ross Sea region) the Hg_T in surface snow is greatly enhanced at the sea ice edge a ent to the freezing ocean surface (Brooks et al., 2008). While Mount Erebus volcano and he Antarctic base of 1200 people may influence higher Hg ocean surface concentrations in the McMurdo region, the Casey station area is only affected by a small human community and Adelie penguin colonies. Note that the Hg concentrations we found in fast ice near Casey station (0.9-28.4 pmol.L^{-1}, Web appendix 2) are also elevated and three orders of magnitude above the ncentration range measured in surface water in the SO. Whilst data from Brooks et al. (2008) and our data point towards an enrichment in Hg in the snow pack, one can expect that a large part of the Hg deposited with snow on the continent and on the sea ice is rapidly re-emitted because of Hg^{II} photo-reduction, as it has been suggested for the Arctic environment (Poulain et al., 4). However, the post-depositional fate of Hg in snow has not yet been assessed near the ice edge, where most of the oxidation of Hg^0 takes place due to halogens released from the sea. The magnitude of the Hg re-emission is still under debate (Larose et al., 2010). Bargagli et al. (2005) found that whilst a large proportion of Hg deposited in surface snow during austral spring MDEs can be efficiently and rapidly recycled back to the atmosphere by photoreduction processes, this process cannot compensate for the total deposition. Dommergue et al. (2010) also concluded that, due to the high reactivity of Hg^0 and the presence of Hg^{II} from late winter to summer, there is likely to be an portant net input of atmospheric Hg onto Antarctic surfaces. Conversely, Chaulk et al. (2011) recently concluded, from a study on mercury transport across the ocean-sea-ice-atmosphere interface in the Arctic Ocean, that the impact of MDEs on Hg concentrations in the sea-ice is insignificant. Climatic differences may be at the origin of this discrepancy. eed, high precipitation rate does occur around the Antarctica coasts on the fringes of the low-pressure systems (up to 80 mm yr^{-1}, http://www.antarctica.ac.uk/met/climate/wmc/). Our observations of high Hg values in snow (Fig. 8d) support the idea of a net atmospheric deposition a the sea ice edge, where halogen oxidation is favoured. The low salinity and warm temperature of the upper sea ice cover implies melting snow events, which also suggest that atmospheric Hg deposition may contribute to the higher concentration of Hg_T in the top most part of the ice cover (Fig. 8). In addition, when the sea ice extent increases in autumn/winter in the SZ, the sea surface is protected from the UV, resulting in decreased Hg^{II} photoreduction, and allowing the build-up of Hg-enriched surface waters during winter months. This process may concur to explain the elevated Hg_T and Hg_R

concentrations we observed in under-ice seawater during the Casey field work and further in the SZ during GEOTRACES cruise (Figs. 3 and 4). The build-up of Hg enriched surface waters under the ice is (i) supported by the low value of the DGHg/Hg_R ratios in surface samples (< 30% in the SZ at the ice edge), which suggests that Hg_R is constituted mainly of oxidized Hg and, (ii) consistent with the presence of dissolved organic ligands exuding from the massive primary production at the basal ice into surface waters (see high POC and Chl*a*, Fig. 8g and h, and web appendix 2). Mercury enrichment from sedimentary sources even in the coastal zone seems unlikely at this time of the year, since, despite the shallow bathymetry, the seawater profiles o not show contribution from sediment resuspension (Fig. 8 and Web appendix 2).

However, such high concentrations in surface waters were also found for iron and other trace elements during the Casey time-series study (van der Merwe et al., in press), metals ich have no locally enhanced atmospheric sources. The under-ice seawater profiles show lower Hg_T concentrations with increasing depth and sampling days (Fig. 8). This spatial and temporal distribution suggests a seeding of Hg_T from melting ice. This process is most likely initiated by the warming of the upper ice cover (van der Merwe et a in press), followed by gravity-driven brine movement and density-driven convection mechanisms at the ice/water interface (brine salinity > seawater salinity). This interpretation agrees with some of the conclusions by Chaulk et al. (2011), who proposed that Hg in the sea-ice Arctic environment is primarily driven by particle enrichment and salt rejection during the sea ice formation. Our results do suggest an exclusion of Hg from ice and its enrichment in brine by the positive relationships found between Hg and salinity in ice and brine (R^2 = 0.69 and 0.48, for Hg_T and Hg_R, respectively), but do not support a role for particles, since we filtered our snow, ice and brine samples.

In summary, we suggest that multiple processes are able to enrich Hg in the surface waters in the seasonal ice zone: (i) a net atmospheric Hg deposition on ice-free surface water near the ice edge, (ii) the shielding from photoreduction under the ice-cover during winter months, (iii) massive algal production at basal sea ice during spring and summer, and (iv), the Hg enrichment in brine during sea ice formation. These processes result in build-up of Hg-enriched surface waters during winter months and its subsequent downward transfer with the AABW. The hypothesis of a Hg enrichment in AABW is supported by the slightly higher Hg_R mean concentration compared to CDW and AAIW, and the slightly higher Hg_T mean concentration compared to AAIW (Tables 1 and 2). The relative contribution of the various processes may vary seasonally and would,

therefore, require further investigations. Indeed in the present observations, we might have some decoupling in the processes between the SZ observations during the SR3 GEOTRACES transect made in autumn (when sea ice is formed) and Casey station observations made during the Austral spring (when sea ice melts).

Regarding methylmercury in the sea ice environment, the complex distribution of $MeHg_T$ distribution in the coastal "snow-sea ice-seawater" continuum (Fig. 8) favours a multiple source system, consistent with the recent findings by Larose al. (2010) who conclude that MMHg is supplied to Arctic environments by various pathways that occur simultaneously. Our observations of high $MeHg_T$ in snow, seawater and basal sea ice (Fig. 8c) suggest that, oceanic and atmospheric methylmercury sources and Hg methylation at the ice-water interface (where sea ice algae are abundant as revealed by the high Chla and POC content) are dominant processes (see section 4.6). Abiotic methylation may occur in th atmosphere (Gardfeldt et al., 2003) as a result of the presence of acetate as methyl donor and Hg^{II} in the atmospheric aqueous phase. Aerobic microbiological and abiotic (*via* DMSP by-products) methylation at the ice pack interfaces are both possible as proposed by Larose et l. (2010) for the snowpack of the Svalbard Archipelago.

5.2. Mercury speciation in SO waters

Although Hg is considered as a reactive element with a short residence time in seawater (similar to Pb), its vertical distribution in the ocea is more complex than simple surface enrichment and low concentrations at depth, reflecting an atmospheric source and particle removal, respectively. Indeed, that fact that several species participate in the oceanic organic matter cycle of generation and mineralization, results in distributions characterized by surface depletion and elevated concentrations at depth in the egeneration zone. The vertical distributions of Hg_R, $MeHg_T$, and DGHg that we found in SO waters are rather "classical", corresponding to the Hg cycle described above. Indeed, the Hg species profiles we recorded in the SO are consistent with the early or refined general model (e.g., Mason and Fitzgerald, 1990; Sunderland et al., 2009), according to which Hg enters the ocean s inorganic species from the atmosphere, is scavenged by particles that sink from the euphotic zone and re-supply Hg at depth during organic matter degradation, and that serve as a substrate for methylating bacteria.

Whereas, Hg_R vertical profiles (Fig. 4) reflect both dry RGHg and t Hg^{II} deposition on the sea surface, and organic matter regeneration processes that mobilize H from biogenic particles, $MeHg_T$ concentrations increase downward (Fig. 5) as a result of methylation-demethylation in the water column with net methylation at depth. The $DGHg/Hg_R$ ratios in surface waters (always < 50%) suggest a significant supply of Hg^{II} *via* atmospheric deposition. $MeHg_T/Hg_T$ ratios, considered as a proxy for net methylation for the water column as well as for sediment (Fitzgerald et al. 2007), were high in the sub-thermocline hypoxic zone (50%) and up to 78% in the sub-thermocline hypoxic zone at Stn. N-05 (Fig. 5c). Malcolm et al. (2004) measured methylation in the thermocline waters of the North Pacific Ocean, and sub-thermocline marine waters enriched with nutrients that stimulated the bacterial community were found to favour Hg methylation. In the Southern Ocean, the phytoplankton ass and export of organic matter from the photic zone is known to be high in AZ and SZ (Sullivan et al., 1993; Sokolov, 2008) and should provide substantial inorganic Hg at depth with the sinking and regeneration of organic particles. Thus, we hypothesize that the hypoxic zone f the AZ of the SO is an area of strong net Hg methylation supported by substantial organic matter regeneration and a large inorganic Hg substrate supply.

It could be argued that the $MeHg_T$ distribution along the SR3 GEOTRACES transect is just the trace of methylated mercury species advected South with the W, and subsequently upwelled as CDW at the Antarctic divergence. Indeed, the distributions of oxygen and $MeHg_T$ are largely mirror images of each other, with maximum values of $MeHg_T$ observed in the oxygen minimum of the upper CDW. The distribution of high $MeHg_T$ waters reflects, in part, the shoaling and poleward spreading of upper CDW. However, advection and mixing alone cannot explain the increase in $MeHg_T$ concentrations to the south. $MeHg_T$ concentrations were high for water layers with potential density ranging between 27.50 and 27.75, and reached maximal values between 58°-63°S, suggesting there must an *in situ* source of $MeHg_T$ at high southern latitudes (Web appendix 4). The AOU distribution, a proxy for heterotrophic activity, showed the highest values for the same isopycnals at the same latitudes (Web app ix 5). This supports the idea of a bacterial methylation of inorganic Hg within the hypox part of the oceanic water column, most significantly in the AZ and SZ. In addition, the lower concentration of $MeHg_T$ observed in the vicinity of the Antarctic continent (Fig. 6) precludes the significant influence of $MeHg_T$ inputs from shelf sediments in the central part of the SZ. Th overall correlation between $MeHg_T$ and

AOU along the SR3 transect is highly significant ($p<0.001$) with an equation: $MeHg_T$ (pmol) = 0.0031*AOU (µmol) + 0.119 (R^2 = 0.722, n = 236). The regression coefficient is of the same order of magnitude as that calculated for the first 600 m of the Mediterranean Sea (Cossa et al., 2009; Heimbürger et al., 2010) and North Pacific (recalculated from the data of figure 4 by Sunderland et al. (2009)), i.e., ~0.004 ($pmol_{MeHg}$/ μmol_{AOU}). Calculated for each station individually, 20 out of a possibility of 27 MeHgT *vs* AOU relationships were significant ($p<0.10$), with 14 highly significant ($p<0.01$) (Web appendix 6). Regression coefficients varied appreciably from one station to another (0.0016 – 0.0051 $pmol_{MeHgT}$ / μmol_{AOU}). Low regression coefficients were observed in the SAZ north of the SAF and high values were observed in the AZ and SZ (web appendix 6). The regression coefficient of the $MeHg_T$ *vs* AOU relationships has been interpreted as a proxy for the *in situ* methylation capacity of the water column per unit of oxygen consumed (Cossa et al., 2009; Heimbürger et al., 2010), and therefore, reflects in some way the bioavailability of Hg for methylating bacteria. Thus, the Hg bioavail ity would be favored in the AZ and SZ of the SO. The enhanced Hg de tion and the unique Hg cycle within the sea ice zone may be responsible for the enhanced Hg bioavailability. The Hg^{II} fraction of the Hg_R, with concentrations several times higher in the SZ than elsewhere, is a good candidate group of species for the bioavailability for methylation. If we extrapolate the observations we made concerning the area under the ice on a coastal site (see above, section 5.1.) to the edge of free sea ice development, a building up of Hg enriched water under the ice in SZ during the polar night may be assumed. In spring and summer with the opening of the pack due to ice melting and the development of phytoplanktonic blooms, inorganic Hg is sorbed and/or taken u by phytoplankton cells provided by the large primary production in the SZ (Sullivan et al., 1993; Sokolov, 2008) and can undergo methylation in the euphotic and/or aphotic zone as proposed by Heimbürger et al. (2010) for the open Mediterranean. This inte tation is supported by the early results from a single 0–200 m profile in the SO (53°30'S; 9°00'E), where both MHg and DMHg have been determined with sub-surface maxima (0.1-0.2 $pmol.L^{-1}$) (Pongratz and Heumann, 1998). Furthermore, the production of methylated Hg by marine polar bacteria has been demonstrated by the same authors in a subsequent study (Pongratz and Heumann, 1999).

5.3. The role of the SO in the global Hg cycle

Mercury is thought to enter the ocean mainly *via* atmospheric deposition. Even if the upper ocean is not in a steady state with the atmosphere, th surface water Hg_T concentrations reflect

the magnitude of the atmospheric Hg deposition (Mason nd Gill, 2005). In spite of the removal processes, namely scavenging and evasion, deep water masses previously in contact with the atmosphere would contain the trace of the atmospheric eposition received when it was at the surface. This has been proposed for the Atlantic ocean water column, where a major portion of the deep water of the World Ocean is formed by the deep convection of surface waters (Mason et al., 1998; Cossa et al., 2004). Indeed, the North Atlantic surface waters sink in the Labrador and Norwegian Seas to form North Atlantic Deep Water (NADW) (Rahmstorf, 2002). This water mass travels South and reaches the SO to form the Circ olar Deep Waters (CDW). In the NADW at 65°N (1000 m), Mason et al. (1998) measured Hg_T concentrations higher than 2 pmol L^{-1}, whereas Cossa et al. (2004) found slightly lower concentrations (~1.7 pmol L^{-1}) in the core of the NADW at a lower latitude (48°N) and at greater depth (2000 m). Traveling South NADW does not seem to change its Hg concentration markedly, since a concentration of 1.8 pmol L^{-1} was recorded by Mason and Sullivan (1999) in the South Atlanti at ~16°S. Our present Hg_T measurements made in the CDW, collected at depths ranging from 500 to 3000 m, far to the East (140°E) and South (46-62°S) are lower, 1.2 ± 0.3 pmol L^{-1} (Table 1), than all the measurements made in the NADW until now. This 1.8 to 1.2 pmol L^{-1} concentration decrease may be attributable to Hg scavenging during the transit of this water mass southward through the Atlantic and eastward in the SO. From the Hg_R distribution in deep waters along the SR3 transect (Fig. 4), it appears that labile Hg concentrations tend to be slightly higher north of 53°S than south, which supports the idea of a scavenging of certain reactive cies of Hg within deep waters during their transit poleward. As shown by the Hg_T distribution on the transect (Fig. 3), it is clear that the Hg originating from the atmosphere in the North Atlantic and brought to the southern hemisphere with NADW is not responsible for the Hg_T enrichment south of the SAF observed on the SR3 transect. More likely, the surface distribution with high concentrations at the southernmost stations suggests an Hg source in the surface water near the ice edge (Fig. 3). These high surface Hg concentrations (> 2 pmol.L^{-1}) were found under sea ice broken by the research vessel (Stns. N-02 and N-03) and at the SPF (St. N-08). The net atmospheric Hg deposition is a likely source for this enrichment. Further Hg transfer to the AABW would be favored by the sea ice formation (excluding Hg with salts), and during the ice melting, which would seed the water column with Hg in the SZ. Based on a difference of mea Hg_T concentrations of 0.16 pmol L^{-1} between AABW and CDW (Table 1) and a flux of AABW sinking around the SO of 5.4 ± 1.7 Sv

(Orsi et al. 2002), a total Hg flux from sea surface to deep ocean of 27 kmol.yr^{-1} during sea ice formation can be derived. The effect of Hg exclusion during ice formation seems insufficient for explaining such flux since an increase of 0.1 salinity unit would only generate a 0.02 pmol L^{-1} change in Hg_T concentration ($Hg_{Tpmol.L}{}^{-1}$ = 0.21*Sal + 3.6, R^2 = 0.69), i.e., ~3.5 kmol.yr^{-1} for 5.4 Sv. Net atmospheric Hg deposition near the sea ice edge would be the additional source.

In contrast with AABW, AAIW formed north of the Antarctic divergence in the PFZ show a slight Hg depletion compared to CDW (Tables 1 and 2). s may be the result of Hg removal processes in surface waters, namely Hg^{II} reduction, which leads to Hg^0 evasion to the atmosphere, and the Hg^{II} sorption onto phytoplankton, which leads to Hg sinking with particles exported to the ocean floor. From this first survey of Hg distribution and speciation, we can reasonably speculate that a part of Hg removed from the SO surface north of the PFZ may be atmospherically transported south, with high-altitude circulation, transferred in the lower troposphere with the polar cell circulation, then carried north to the MBL with katabatic winds. Near the sea ice edge atmospheric Hg undergoes oxidation notably during MDE, to be reinjected into the deep ocean in the SZ due to the sea ice formation-melting cycle.

In summary, our findings, placed within the context of global oceanic Hg_T distribution, imply a (i) removal of Hg by settling particles from NADW on its way to the Southern Ocean, (ii) an evasion of Hg from the sea surface North of the convergence zone, and (iii) an Hg enrichment of the waters in the SZ, which spread off with the AABW t ling northward. This Hg enrichment would have its source in the MBL south of the SACCF, near the ice-edge (within the SZ) and would be transferred to depth by sinking of dense wate formed by brine rejection during sea ice formation. Further confirmation of differences in Hg c entration between water types is necessary before concluding to a model where the Hg atmospheric injection and redistribution mechanisms acting in the SO lead to a transfer north w AABW of Hg enriched waters.

6. CONCLUSIONS

With 50% of the values (the interquartile range) lying between 1.1 and 1.5 pmol.L^{-1}, Hg_T concentrations in the water samples collected along the SR3 GEOTRACES transect between the Antarctic continent and Tasmania are within the picomo range, consistent with other recent measurements performed in the Global Ocean (Mason and ullivan, 1999; Laurier et al., 2004;

Cossa et al., 2004; Cossa et al., 2009; Sunderland et 2009). Nevertheless, some unique features in the Hg species distributions are clearly noticeable. Firstly, the concentration of Hg_T and Hg_R in surface waters increases poleward, reaching values > 2 pmol.L^{-1} in the AZ and SZ, and a maximum of 44.4 pmol.L^{-1} below the coastal sea ice. Secondly, Hg_T, Hg_R and $MeHg_T$ concentrations tend to be higher in the AABW compared the AAIW, and thirdly, high proportions of methylated mercury (50%) occur in the hypoxic part of the water column, up to 78% in AZ. These distribution characteristics suggest ree main drivers of the SO Hg cycle: (i) a net Hg input to the ocean surface near the Antarctic c nent from an atmospheric source, (ii) a role of sea ice formation in the transfer of Hg enriched waters to depth, and (iii) a substantial net methylation of Hg south of the SPF as a result of the co-location of enhanced atmospheric Hg^{II} input and the bacterial decomposition of organic matte produced by intense phytoplankton blooms, which are superimposed with the advection of m ylmercury-enriched deep water by the upwelling at the Antarctic divergence.

High Hg concentrations have been observed in Antarctic biota, despite the remoteness from anthropogenic sources (Bargagli, 2008; Bargagli et al., 2005). Birds from the SO have very large Hg concentrations (up to 680 µg g^{-1}, wet weight) (Hindell et al., 1999), suggesting a huge bioaccumulation, surprising *a priori* for a remote environment. In order to be biomagnified in fish and sea-birds, inorganic Hg must first be converted to methylm ury and bioconcentrated by phyto- and zoo-plankton. Our first systematic measurement of $MeHg_T$ in Antarctic waters suggests that a unique combination of atmosphere, ocean and sea ice processes can explain the elevated concentrations of methylmercury observed in the AZ and SZ of the remote Antarctic waters (including the sea ice zone), and therefore, th high bioaccumulation of Hg in pelagic seabirds, marine mammals and top predators. Halogens released to the atmosphe during sea ice formation facilitate the oxidation and deposition of atmospheric Hg; extensive phytoplankton blooms in the same region produce organic particles that scavenge inorganic Hg from the water column and sink to supply organic matter and inorganic Hg as a substrate for methylating bacteria in the hypoxic zone; and the upwelling of wat that is low in oxygen and rich in $MeHg_T$ (both characteristics resulting from bacterial activity during the long transit time of the upper CDW) further enhances $MeHg_T$ concentrations. As a result, the remote Antarctic waters exhibit some of the highest $MeHg_T$ concentrations observed in the open ocean, notably within the AZ and SZ. In the North Pacific, Hg levels in both predators and prey have been found to increase

with depth, as does the concentration of methylated Hg in seawater (Choy et al., 2009). This association between Hg levels in organisms and in their ambient environment, together with our observations of highly elevated $MeHg_T$ concentrations in Antarctic waters, suggest that Antarctic marine biota are exposed to high levels of $MeHg_T$, deriving from both natural and anthropogenic sources of atmospheric-borne inorganic Hg methylated *in situ*, and oceanic preformed methylated species, advected with CDW. As fishing activities exte to more remote regions, including Antarctica, the presence of high $MeHg_T$ concentrations in Antarctic waters may have important implications for the health of human consumers.

ACKNOWLEDGEMENTS

Thanks are due to Mark Rosenberg and Alicia Navidad, Mark Rayner, Carrie Bloomfield and Laura Herraiz Borreguero for hydrochemistry analyses and data quality control. This research has been supported by the Australian Antarctic Science projects 2793 and 2900, the Australian Antarctic Division, the Australian Government (ACE CRC) and IFREMER International Division. This work contributes to the Australian Climate Change Science Program and the ternational Polar Year (CASO and GEOTRACES). We thank the captain and crew of R/SV "Aurora Australis". Thanks are also due to NIWA for use of the non-contaminating rosette and Niskin bottles.

REFERENCES

Ariya P. A., Khalizov A. and Gidas A. (2002) Reaction of gaseous mercury with atomic and molecular halogens/ Kinetics, product studies, and atmospheric implica . *J. Phys. Chem. A* **106**, 7310-7320.

Bargagli R., Agnorelli C., Borghini F. and Monaci F. ( ) Enhanced Deposition and Bioaccumulation of Mercury in Antarctic Terrestrial Ecosystems Facing Coastal Polynya. *Environ. Sci. Technol.* **39**, 8150-8155.

Bargagli R. (2008) Environmental contamination in Antarctic ecosystems. *Sci. Total Environ*. **400**, 212-226.

Black F. J., Conaway C. H. and Flegal A. R. (2009) Stability of Dimethyl Mercury in Seawater and Its Conversion to Monomethyl Mercury. *Environ. Sci. Technol*. **43**, 4056-4062, 10.1021/es9001218.

Bowie A. R., Lannuzel D., Remenyi T. A., Wagener T., Lam P. J., Boyd P. W., Guieu C., Townsend A. T. and Trull T. W. (2009) Biogeochemical iron budgets of the Southern Ocean south of Australia: Decoupling of iron and nutrient cycles in the subantarctic zone by the summertime supply. *Global Biogeochem. Cycles* **23**, 1-14 GB4034, doi:10.1029/2009GB003500.

Brooks S., Lindberg S., Southworth G., and Arimoto R. (2008) Springtime atmospheric mercury speciation in the McMurdo, Antarctica coastal region. *Atmos. Environ.* **42**, 2885-2893.

Bruland K. W. and Lohan M. C. (2003) *Control of Trace Metal in Seawater*. Chap. 6.02. p:23-47. In: Treatise on Geochemistry, Vol. 6 (The Oceans and Marine Geochemistry). Holland, H. D. and. Turekian K. K. Elsevier.

Chaulk A., Stern G. A., Armstrong D., Barber D. G., and Wang F. (2011) Mercury Distribution and Transport Across the Ocean-Sea-Ice-Atmosphere Interface in the Arctic Ocean. *Environ. Sci. Technol.* Dx.doi.org/10.1021/es103434c.

Choy C. A., Popp B. N., Kaneko J. J. and Drazen J. C. (2009) The influence of depth on mercury levels in pelagic fishes and their prey. *PNAS* **106**, 13865-13869.

Cossa D., Martin J.-M., Takayanagi K. and Sanjuan J. (1997) The distribution and cycling of mercury species in the western Mediterranean. *Deep Sea Res. II* **44**, 721-740.

Cossa D., Cotte-Krief M. H., Mason R. P. and Bretaudeau-Sanjuan J. (2004) Total mercury in the water column near the shelf edge of the European continental margin. *Mar. Chem.* **90**, 21-29.

Cossa D. and Coquery M. (2005) *The Mediterranean Mercury Anomaly, a Geochemical or a ogical Issue.* p. 177-208. In: The Mediterranean Sea, A. Saliot editor. The Handbook of Environmental Chemistry, Vol. 5, Water Pollution, Part K. Springer-Verlag, Berlin-Heidelberg. 413pp.

Cossa D., Averty B. and Pirrone N. (2009) The origin of methylmercury in open Mediterranean waters. *Limnol. Oceanogr.* **54**, 837-844.

Cowley R. (1999) *Hydrochemistry operations manual*. CSIRO Marine Laboratories Report 236. CSIRO Marine Research, Melbourne.

Dommergue A., Sproveri F., Pirrone, N., Ebinghaus R., Brooks S., Courteaud J. and Ferrari C. (2010) Overview of mercury measurements in the Antarctic trop here. *Atmos. Chem. Phys.*, **10**, 3309-3319.

Ebinghaus R., Kock H. H., Temme Ch., Einax J. W., Löwe A. G., Richter A., Burrows J. P. and Schroeder W. H. (2002) Antarctic Springtime Depletion of Atmospheric Mercury. *Environ. Sci. Technol.* **36,** 1238-1244.

Eicken H. (1992) Salinity profiles of Antarctic sea ice: field data and model results. *J. Geophys Res*. **97** (C10), 15545-15557.

Fitzgerald W. F. and Lamborg C. H. (2003) *Geochemistry of Mercury in the Environment*. In: Treatise of Geochemistry, Turekian K. K. editor. Vol. 9. p. 107-148. Elsevier.

Fitzgerald W. F., Lamborg C. H. and Hammerschmidt C. R. (2007) M ine biogeochemical cycling of mercury. *Chem. Rev*. **107**, 641-662, 10.1021/cr050353m.

Garfeldt K., Munthe J., Strömberg D. and Lindqvist O. (2003) A kinetic study on the abiotic methylation of divalent mercury in aqueous phase. *Sci. Total Environ*. **304**, 127-136.

Grasshoff, K. (1976) *Methods of seawater analysis*. Verlag Chemie, Weinheim.

Gobeil C., Macdonald R. W. and Smith J. N. (1999) Merc Profiles in Sediments of the Arctic Ocean Basins. *Environ. Sci. Technol*. **33**, 4194-4198.

Heimbürger L.-E., Cossa D., Marty J.-C., Migon C., Averty B., Dufour A. and Ras J. (2010) Methyl mercury distributions in relation to the presence of n and picophytoplankton in an oceanic water column (Ligurian Sea, North-western Mediterranean). *Geochim. Cosmochim. Acta,* **74**, 5549-4459.

Hindell M. A., Brothers N. and Gales R. (1999) Mercury and cadmium concentrations in the tissues of three species of southern albatrosses. *Polar Biol.* **22**, 102-108.

Horvat M., Kotnik J., Logar M., Fajon V., Zvonaric T. and Pirrone N. (2003) Speciation mercury in surface and deep-sea waters in the Mediterranean Sea. *Atmos. Environ.* **37**, 93-108.

Knapp, G. P., Stalcup M. and Stanley R. J. (1990) *Automated oxygen titration and salinity determination.* Woods Hole Oceanographic Institute Technical Report WHOI–90–35.

Kotnik O., Horvat M., Tessier E., Ogrinc N., Monperrus M., Amouroux D., Fajon V., Gibicar D., Žižek S., Sprovieri F. and Pirrone N. (2007) Mercury speciation in surface and deep waters of the Mediterranean Sea. *Mar. Chem*., **107,** 13- 30.

Lamborg C. H., Tseng C. M., Fitzgerald W. F., Balcom P. H. and Hammerschmidt C. R. (2003) Determination of the Mercury Complexation Characteristics of Dissolved Organic Matter in Natural Waters with "Reducible Hg" Titrations. *Environ. Sci. Technol.* **37,** 3316–3322.

Lannuzel D., de Jong J. T. M., Schoemann V., Trevena A., Tison J.-L. and Chou L. (2006) Development of a sampling and flow injection analysis technique for iron determination in the sea ice environment. *Anal. Chim. Acta* **556**, 476-483.

Lannuzel D., Schoemann V., de Jong, J. T. M., Chou L., Delille B., Becquevort S. and Tison J.-L. (2008) Iron study during a time series in the western Weddell pack ice. *Mar. Chem*. **108**, 85-95.

Lannuzel D., Schoemann V., Pasquer B., van der Merwe P. and Bowie A. (2010) Distribution of dissolved iron in Antarctic sea ice: spatial, seasonal and inter-annual variability. *J. Geophys. Res. Biogeo.* **115**, G03022, doi:10.1029/2009JG001031.

Lannuzel D., Bowie A. R., van der Merwe P., Townsend A d Schoemann V. (2011) Distribution of dissolved and particulate metals in Antarctic sea ice. *Mar. Chem.* DOI : 10.1016/j.marchem. 2011.01.004.

Larose C., Dommergue A., De Angelis M., Cossa D., Averty B., Marusczak N., Soumis N., Schneider D. and Ferrari C. (2010) Springtime changes in snow chemi lead to new insights into mercury methylation in the Arctic. *Geochim. Cosmochim. Acta* **74**, 6263-6275.

Laurier F. J. G., Mason R. P., Gill G. A. and Whalin L (2004) Mercury distributions in the North Pacific Ocean – 20 years observations. *Mar. Chem.* **90**, 3-19.

Lindberg S. E., Brooks S., Lin C.-J., Scott K., Meyers T., Chambers L., Landis M. and Stevens R. (2001) Formation of reactive gaseous mercury in the Arctic: evidence of oxidation of Hg^0 to gas phase Hg^{II} compounds after Arctic sunrise. *Water Air Soil Pollut. Focus* **1**, 295-302.

Lindberg S. E., Brooks, S., Lin C.-J., Scott K. J., Landis M. S. D., Stevens, R. K., Goodsite M. and Richter A. (2002) Dynamic oxidation of gaseous mercury in the Arctic troposphere at polar sunrise. *Environ. Sci. Technol.* **36**, 1245-1256.

Malcolm E. C., Tuit C. B., Jayakumar A. D. and Morel F. M. M. (2004) Investigation o mercury methylation by bacteria in the open ocean. In 7th Intern. Conf. On Mercury as a Global pollutant. *RMZ-Materails and Geoenvironment* **51**, 1193-1194 (Abstract).

Mason R. P. and Fitzgerald W. F. (1990) Alkylmercury species in the Equatorial Pacific. *Nature* **347**, 457-459.

Mason, R. P. and Fitzgerald W. F. (1993) The distribution and biogeochemical cycling of mercury in the Equatorial Pacific-Ocean. *Deep Sea Res. I* **40**, 1897-1924.

Mason R. P., Rolfhus K. R. and Fitzgerald W. F. (1998) Mercury in the North Atlantic. *Mar. Chem.* **61**, 37-53.

Mason R. P., Lawson N.M. and Sheu G.-R. (2001) Mercury in the Atlantic Ocean: Factors contr g air-sea exchange of mercury and its distribution in the upper waters. *Deep-Sea Res. II* **48**, 2829-2853.

Mason R. P. and Sullivan K. A. (1999) The distribution and speciation of mercury in the South and equatorial Atlantic. *Deep-Sea Res. II* **46**, 937-956.

Mason R. P. and Gill G. A. (2005) *Mercury in the Marine Environment*. Chap 10. In: Mercury Sources, Measurements, Cycles, and Effects. Parsons M. B. and P ival J. B. editors. Mineralogical Association of Canada. Short Course, Series Volume 34, Halifax, Nova Scotia, Canada, p. 179-216.

Nakawo M. and Sinha N. K. (1981) Growth rate and salinity profile of first-year sea ice in the Arctic. *J. Glaciol*. 27, 315-330.

Orsi A. H., Whitworth T. and Nolin W. D. (1995) On the meridional extent and fronts of the Antarctic Circumpolar Current. *Deep Sea Res. I* **42**, 641-673.

Orsi A. H., Smethie W. M. and Bullister J. B. (2002) On the total input of Antarctic waters to the deep ocean: A preliminary estimate from chlorofluorocarbon measurements. *Journal of Geophysical Research* 107(C8):3122.

Parker J. L. and Bloom N. S. (2005) Preservation and storage techniques for low-level aqueous mercury speciation. *Sci. Total Environ*. **337**, 253-263.

Pongratz R. and Heumann K.G. (1998) Determination of c entration profiles of methyl mercury compounds in surface waters of polar and other remote eans by GC-AFD. Intern. *J. Environ. Anal. Chem*. **71**, 41-56.

Pongratz R. and Heumann K.G. (1999) Production of meth ed mercury, lead and cadmium by marine bacteria as a significant natural source for atmospher heavy metals in polar regions. *Chemosphere* **39**, 89-102.

Poulain A. J., Lalonde J. D., Amyot M., Shead J. A., Raaofie F. and Ariya P.A. (2004) Redox transformations of mercury in an Arctic snowpack at springtime. *Atmos. Environ*. **38**, 6763-6774.

Rintoul S. R. (2006) *Circumpolar Deep Water*. pp. 240-242, In: Encyclopedia of the Antarctic, Routledge, New York,.

Rintoul S. R. and Bullister J. (1999) A late winter hydrographic section between Tasmania and Antarctica. *Deep Sea Res. I* **46**, 1417-1454.

Schroeder W. H., Anlauf K. G., Barrie L. Y., Lu A., Schneebeerger D. R. and Berg T. (1998) Arctic springtime depletion of mercury. *Nature* **394,** 331-332.

Sedwick P. N., Edwards P. R., Mackey D. J., Grif?ths F. B., Parslow J. S. (1997) Iron and manganese in surface waters of the Australian subantarctic region. *Deep Sea Res. I,* **44**, 1239–1253.

Slemr F., Junkermann W., Schmidt R. W. H. and Sladkovi (1995) Indication of change in global and regional trends of atmospheric mercury concentrations. *Geophys. Res. Lett.* **22**, 2143-2146.

Soerensen, A. L., Skov H., Jacob D. J., Soerensen B. T and Johnson M. S. (2010) Global Concentrations of Gaseous Elemental Mercury and Reactive Gaseous Mercury in the Marine Boundary Layer. *Environ. Sci. Technol*. **44**, 7425-7430.

Sokolov S. (2008) Chlorophyll blooms in the Antarctic Zone south of Australia and New Zealand in reference to the Antarctic Circumpolar Current fronts and sea ice forcing. *J. Geophys. Res. Oceans* **113**, C3, Article Number C03022.

Sokolov S. and Rintoul S. R. (2002) The structure of S hern Ocean fronts at 140E. *J. Mar. Syst.* **37**, 151-184.54.

Sokolov S. and Rintoul S. R. (2007) Multiple jets of the Antarctic Circumpolar Current south of Australia. *J. of Phys. Oceanogr*. **37**, 1394-1412.

Sproveri F., Pirrone N. and Hedgecock I. M. (2002) Intensive atmospheric measurements at Terra Nova Bay in Antarctica during November and December 2000. *J. Geophys. Res*. **107** (D23), 4722-4729.

Stoichev T., Martin-Doimeadios, R. C. R., Tessier, E., Amouroux, D., and Donard, O. F. X. (2004) Improvement of analytical performances for mercury speciation by on-line derivatization, cryofocussing and atomic fluorescence spectrometry. *Talanta* **62**, 433-438.

Sullivan C. W., Arrigo K. R., Mcclain C. R., Comiso J. C. and Firestone J. (1993) Distributions of phytoplankton blooms in the Southern Ocean. *Science* **262**, 1832-1837.

Sunderland E. M., Krabbenhoft D. P., Moreau J. W., Strode S. A. and Landing W. M. (2009) Mercury sources, distribution, and bioavailability in the North Pacific Ocean: Insights from data and models. *Global Biogeo. Cycles* **23**, 14, Gb201010.1029/2008gb003425.

Sunderland E. M. and Mason R. P. (2007) Human impacts on open ocean mercury concentrations. *Global Biogeo. Cycles* **21**, 1-15. doi:10.1029/2006GB002876.

Temme C., Einax J. W., Ebinghaus R. and Schroeder W. H 003) Measurements of Atmospheric Mercury Species at a Coastal Site in the Antarctic and Over the South Atlantic Ocean During Polar Summer. *Environ. Sci. Technol.* **37**, 22-31.

van der Merwe P., Lannuzel D**.**, Bowie A. R. and Meiners K. M. (2011) High temporal resolution observations of spring fast-ice melt and seawater iron enrichment in East Antarctica. *J. Geophys. Res. Biogeo.*, in press.

Weeks W. F. and Ackley S. F. (1986) *The growth, structure and properties of sea ice*. pp. 9-164. In: The Geophysics of sea ice, Untersteiner N. editor. NATO ASI series.

TABLES

Table 1. Summary statistics for Hg_T, Hg_R and $MeHg_T$ concentrations in various water masses of the SO. CDW: Circumpolar Deep Water (salinity >34.6, depth 500-3000m); AAIW: Antarctic Intermediate Water (34.10-34.60; 2-5°C); AABW: Antarctic Bottom Water (34.65-34.75 and <1°C). Mean ± standard deviation, minimum and maximum in brackets and number of samples in italics.

	Hg_T	Hg_R	$MeHg_T$	DGHg
CDW	1.19 ± 0.27 (0.95-1.80) *11*	0.39 ± 0.08 (0.21-0.55) *25*	0.48 ± 0.18 (0.09-0.77) *30*	0.22 ± 0.07 (0.10-0.31) *13*
AAIW	1.15 ± 0.22 (0.82-1.56) *10*	0.38 ± 0.11 (0.14-0.64) *24*	0.44 ± 0.17 (0.04-0.86) *31*	0.24 ± 0.03 (0.21-0.29) *8*
AABW	1.35 ± 0.39 (0.98-1.99) *14*	0.48 ± 0.23 (0.28-1.31) *16*	0.52 ± 0.11 (0.15-0.68) *19*	0.24 ± 0.04 (0.20-0.30) *6*

Table 2. T-test. Probabilities for the significance of the differ s in mean concentration between various water masses. (*) Significant differen at 85% confidence; (**) Significant differences at 95% confidence level.

	Hg_T	Hg_R	$MeHg_T$	DGHg
AABW *vs* AAIW	0.1277*	0.1205*	0.0397**	0.8543
AABW *vs* CDW	0.2170	0.1372*	0.3088	0.6047
AAIW *vs* CDW	0.7772	0.7954	0.3393	0.4456

Figures

Figure 1 : Sampling stations along the SR3 CASO-GEOTRACES transect 879 in the Southern Ocean.

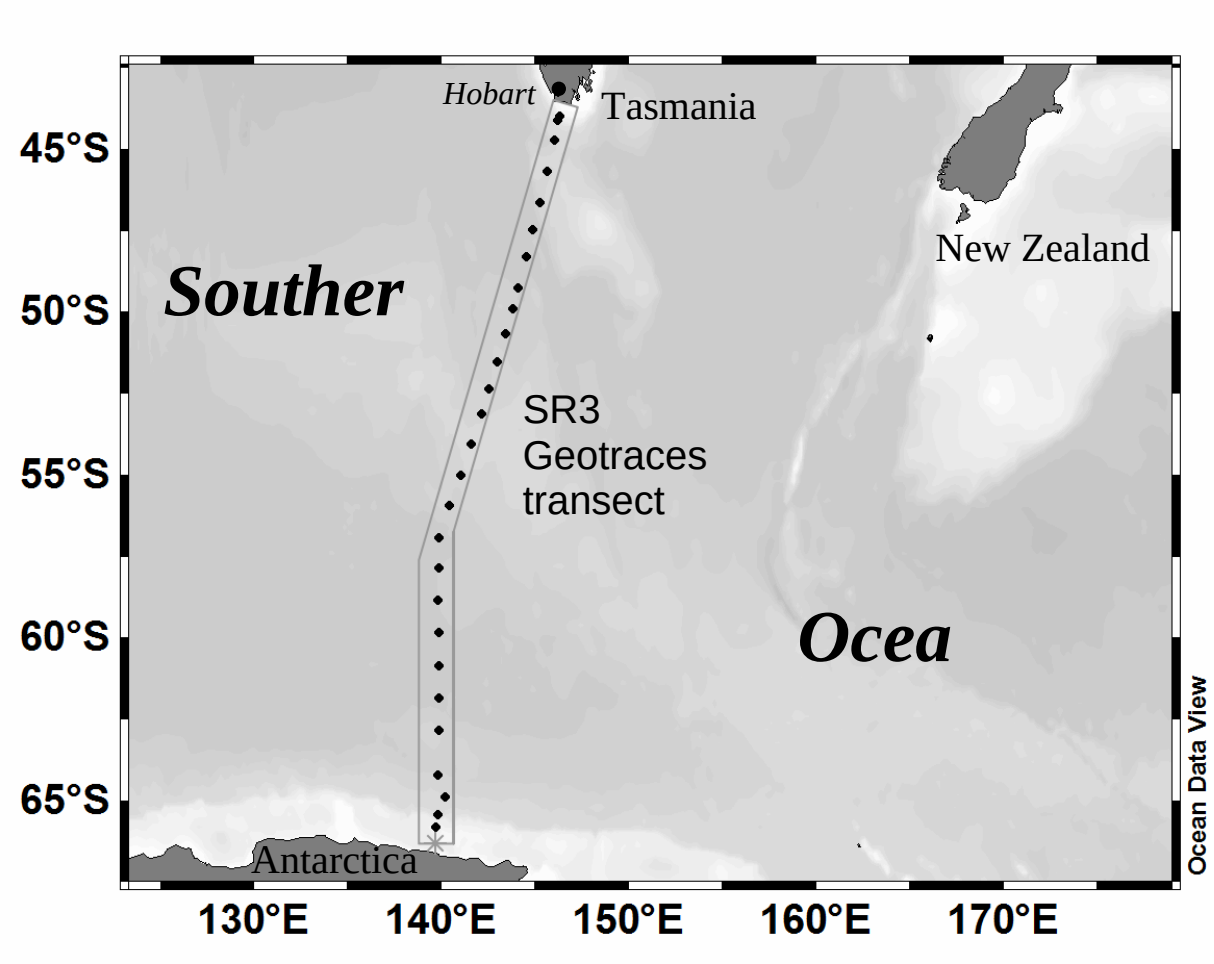

Figure 2 : Distributions of (a) potential temperature (Tpot-0), (b) salinity, (c) phosphate (PO4) and (d) dissolved oxygen along the of the SR3 CASO-GEOTRACES transect in the Southern Ocean.

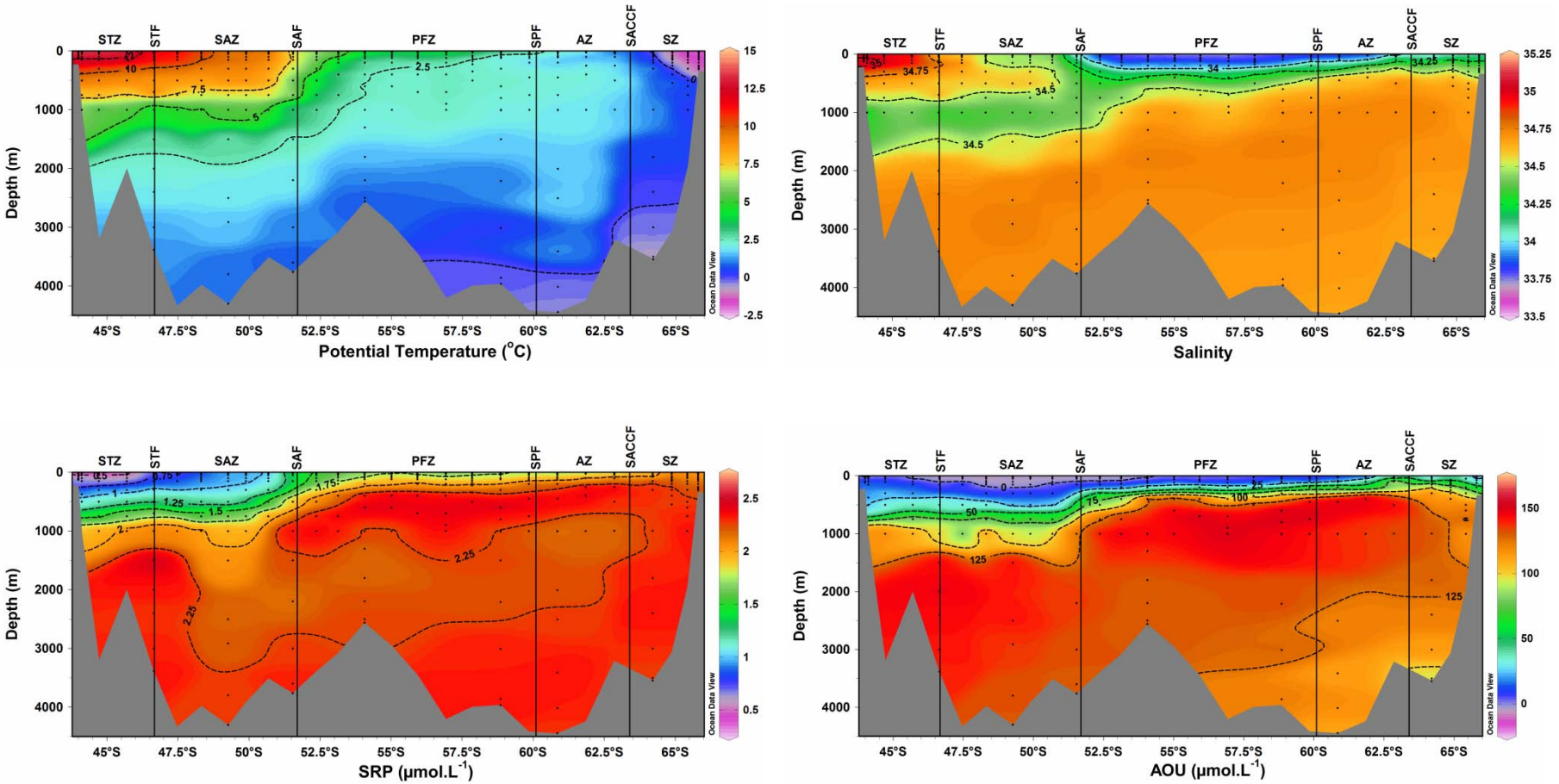

Figure 3 : Total mercury (HgT) distribution along the SR3 CASO-GEOTRACES transect in the Southern Ocean.

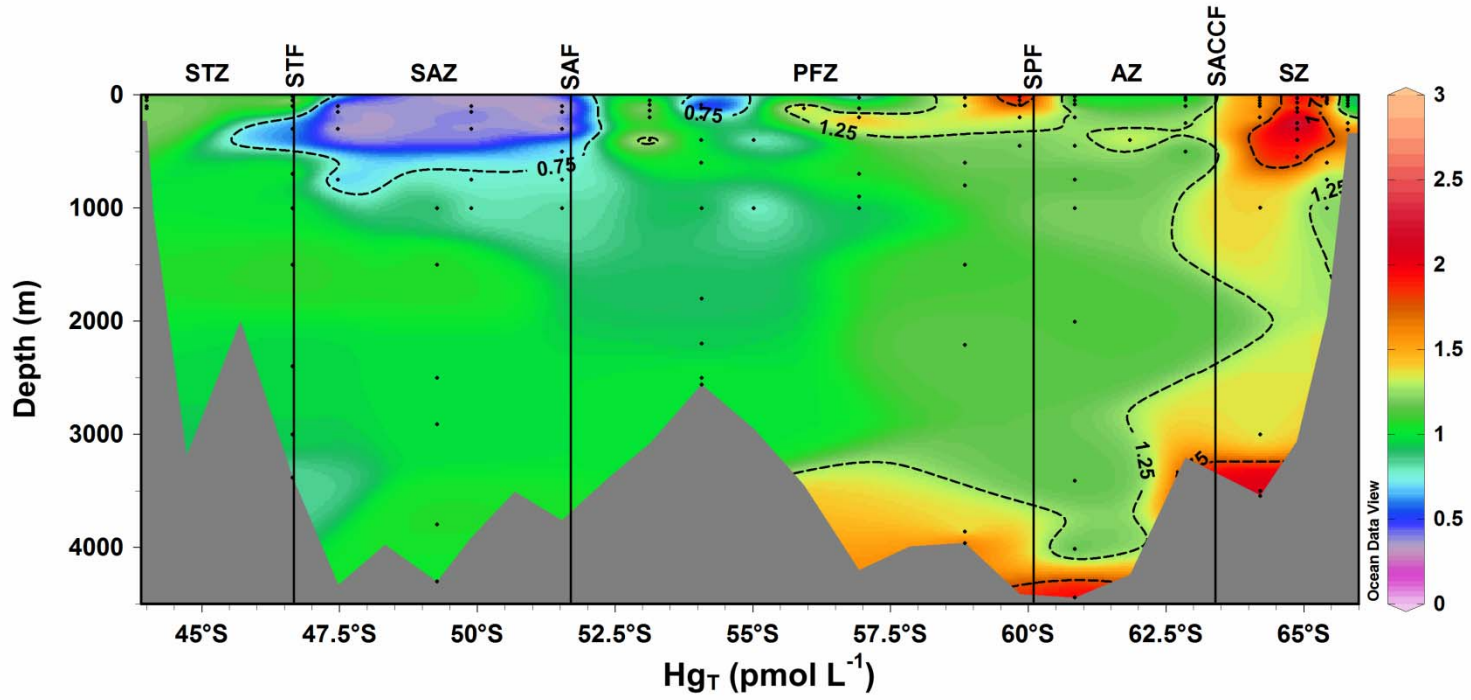

Figure 4 : Total mercury (HgR) distribution along the SR3 CASO-GEOTRACES transect in the Southern Ocean.

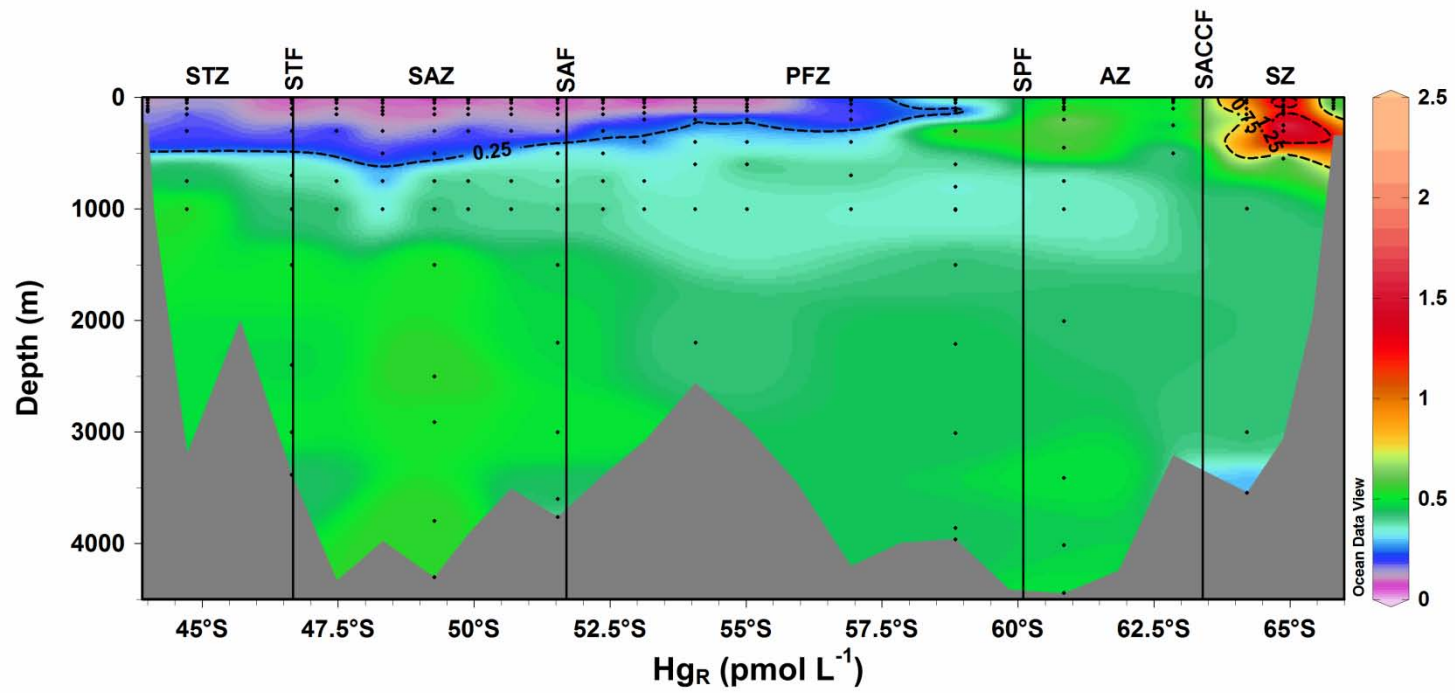

Figure 5 : Vertical distributions of methylated mercury species (MeHgT) along the SR3 CASO GEOTRACES transect in the Southern Ocean. (a) deep profiles, (b) upper ocean profiles, (c) MeHgT/HgT ratio profiles.

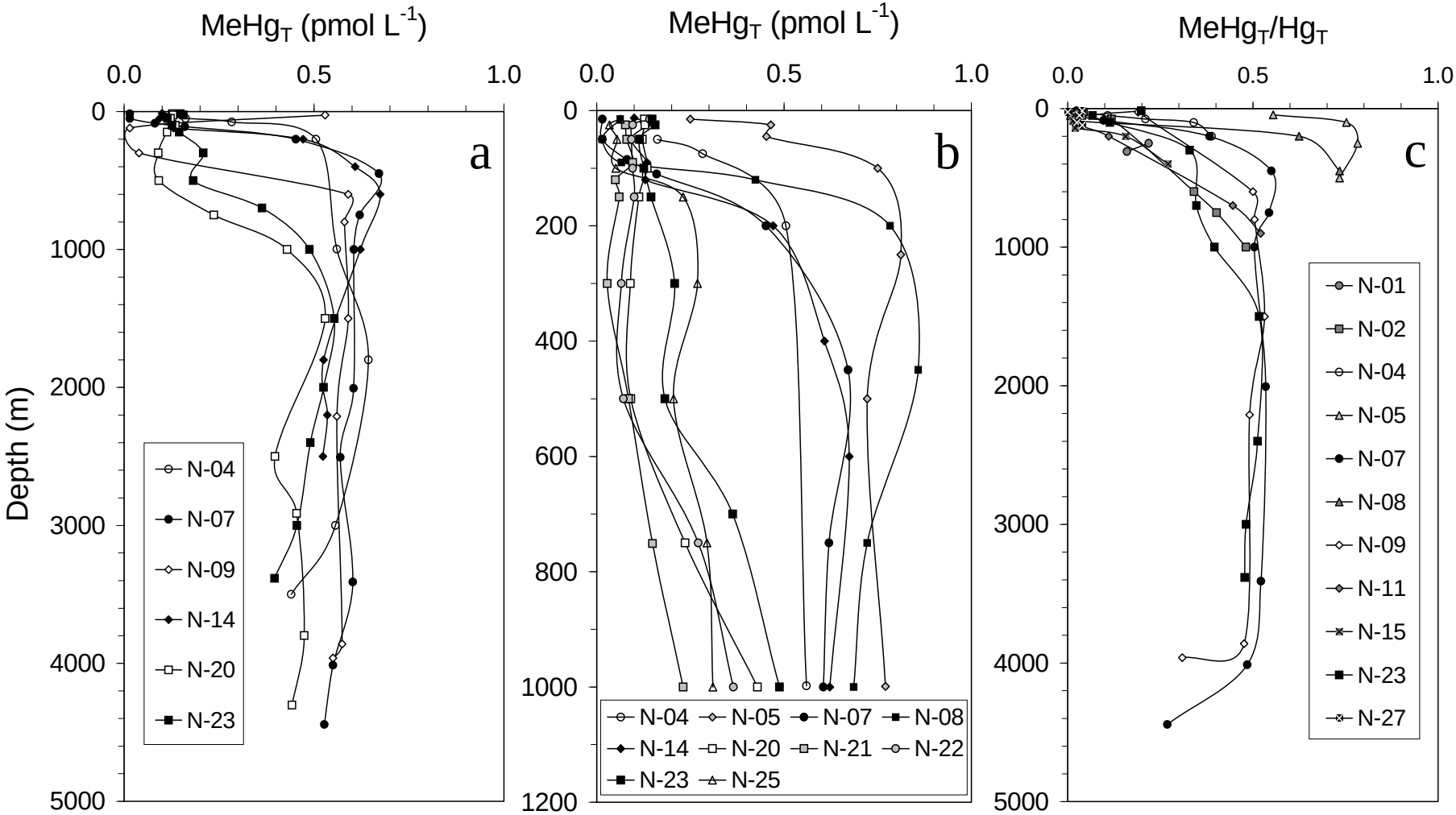

Figure 6 : Methylated mercury species (MeHgT) distribution along the SR3 CASO-GEOTRACES transect in the Southern Ocean.

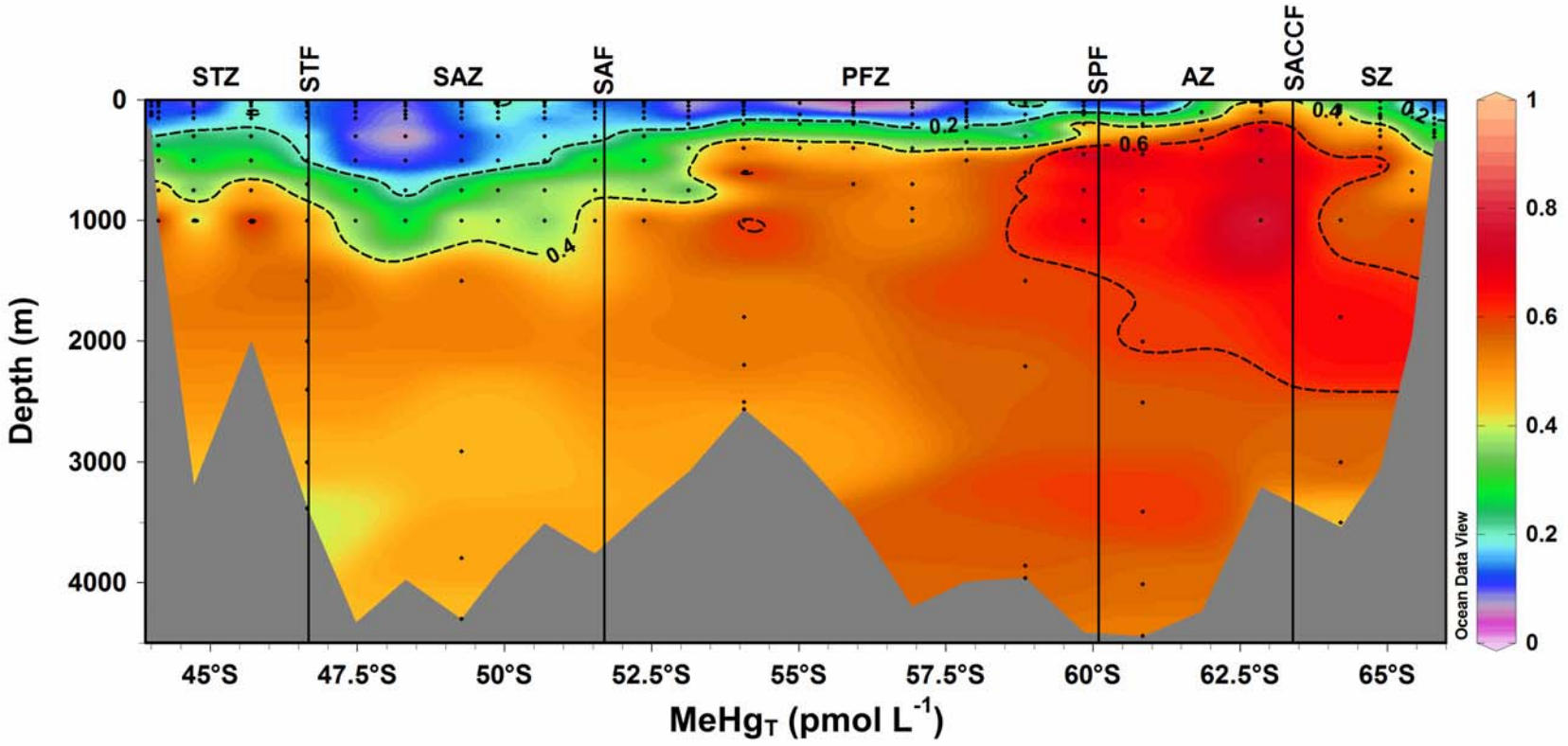

Figure 7 : Vertical distribution of dissolved gaseous mercury (DGHg) along the SR3 CASO GEOTRACES transect in the Southern Ocean.

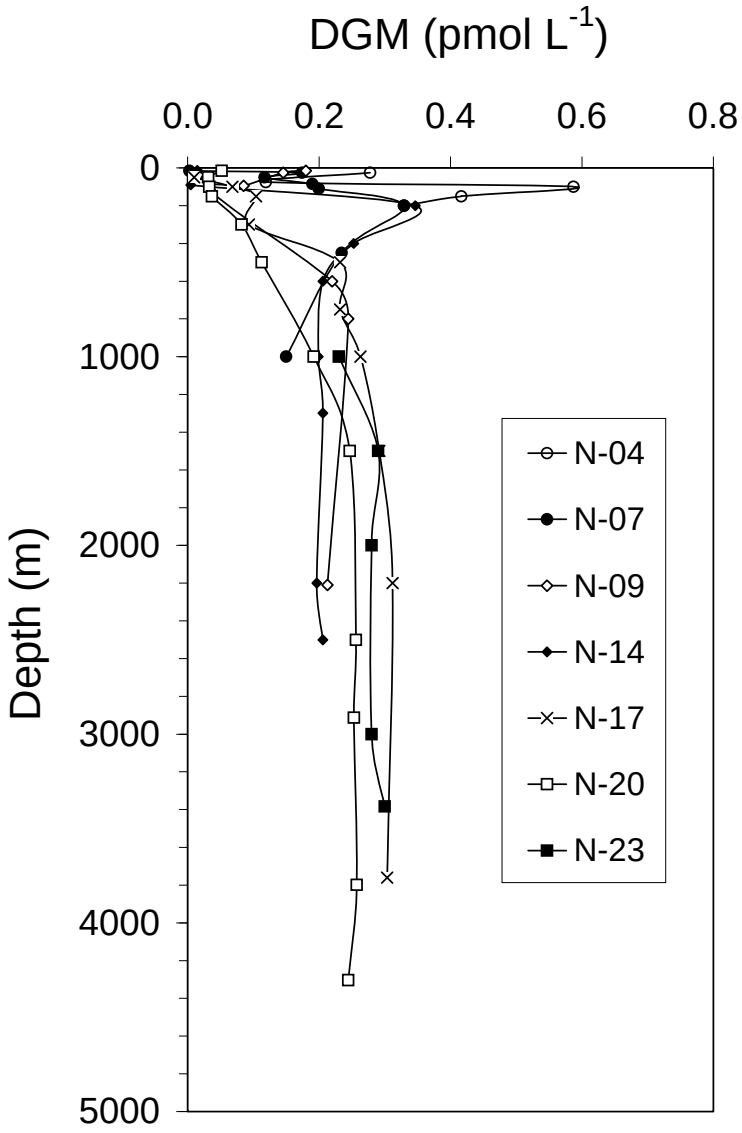

Figure 8 : Vertical distributions of Hg species in snow, bulk sea ice and seawater in the coastal sea ice environment 12 km northeast of the Casey Station (Australian East Antarctic sector) (66°13'S; 110° 39'E). Figures "a" to "e" referee to the snow and sea ice continuum, figures "f" to "j"referee to seawater.

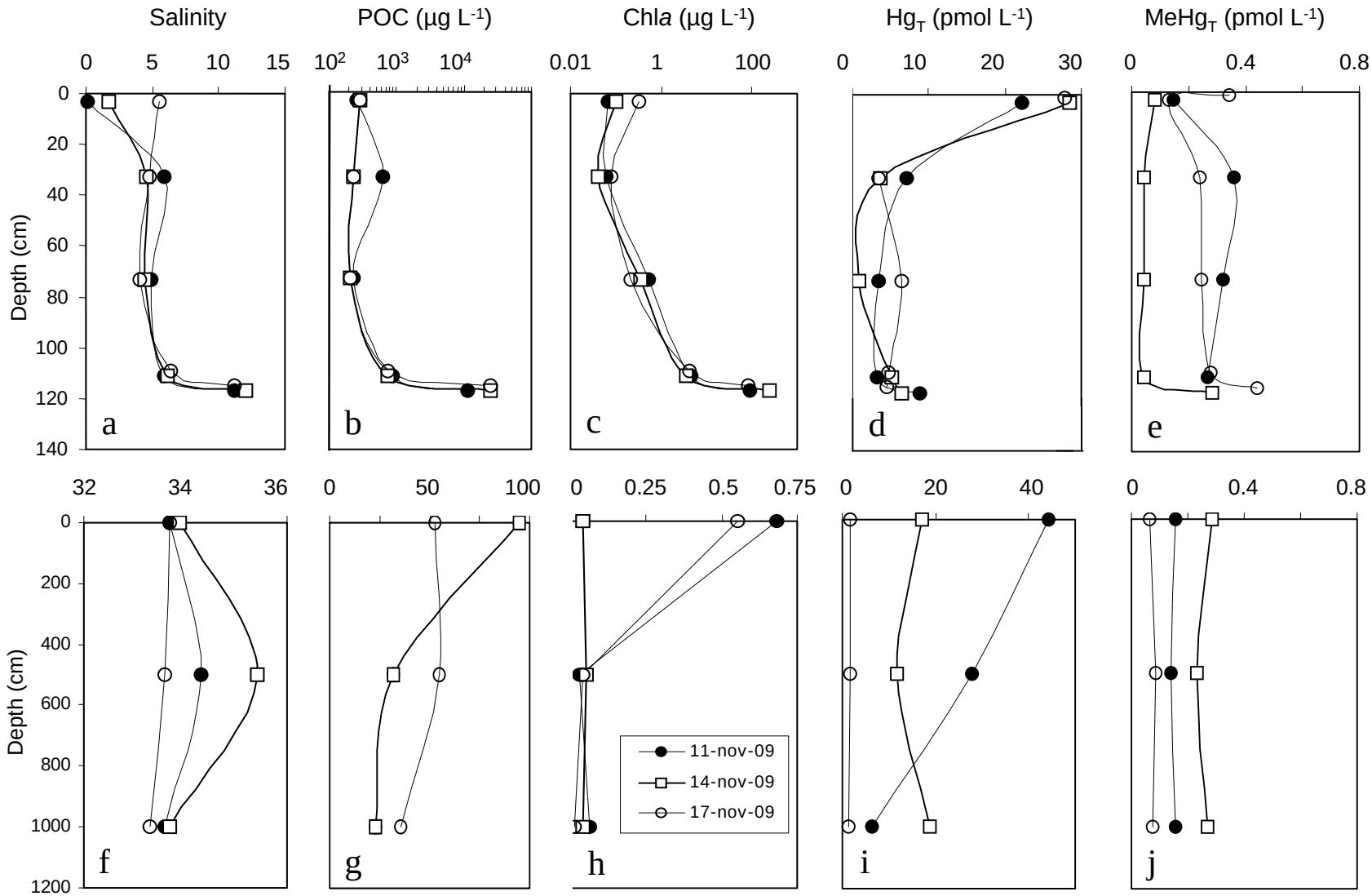

ELECTRONIC ANNEXES

Electronic annex 1. Sampling dates and positions along the SR3 CASO-GEOTRACES transect in the Southern Ocean from Adelie Land (Antarctic continent) and Tasmania (Australia). Stations with ice-pack cover are indicated in italics.

Station	Date (dd/mm/yy)	Position (Lat., Long.)	Sea bottom depth (m)
N-01	*28/03/2008*	*65° 48.19' S, 139° 40.81' E*	*338*
N-02	*29/03/2008*	*65° 25.58' S, 139° 50.61' E*	*1000*
N-03	*30/03/2008*	*64° 52.71' S, 140° 12.63' E*	*3061*
N-04	31/03/2008	64° 12.45' S, 139° 50.47' E	3547
N-05	31/03/2008	62° 51.28' S, 139° 51.48' E	3210
N-06	01/04/2008	61° 50.99' S, 139° 50.88' E	4240
N-07	02/04/2008	60° 51.02' S, 139° 51.13' E	4243
N-08	02/04/2008	59° 50.93' S, 139° 51.57' E	4415
N-09	03/04/2008	58° 51.04' S, 139° 50.31' E	3962
N-10	04/04/2008	57° 51.01' S, 139° 51.10' E	3993
N-11	04/04/2008	56° 55.77' S, 139° 51.04' E	4200
N-12	05/04/2008	55° 55.76' S, 140° 24.56' E	3450
N-13	06/04/2008	55° 01.21' S, 141 01.12' E	2953
N-14	06/04/2008	54° 04.18' S, 141° 36.14' E	2560
N-15	07/04/2008	53° 07.90' S, 142° 08.30' E	3077
N-16	08/04/2008	52° 22.17' S, 142° 32.05' E	3391
N-17	10/04/2008	51° 32.37' S, 142° 59.73' E	3761
N-18	10/04/2008	50° 40.89' S, 143° 25.16' E	3506
N-19	11/04/2008	49° 53.49' S, 143° 48.03' E	3914
N-20	12/04/2008	49° 16.20' S, 144° 05.96' E	4216
N-21	12/04/2008	48° 19.19' S, 144° 31.81' E	3975
N-22	13/04/2008	47° 28.32' S, 144° 54.07' E	4330
N-23	13/04/2008	46° 39.00' S, 145° 14.91' E	3383
N-24	14/04/2008	45° 41.99' S, 145° 39.45' E	2000
N-25	14/04/2008	44° 43.20' S, 146° 03.06' E	3193
N-26	15/04/2008	44° 07.09' S, 146° 13.37' E	1040
N-27	15/04/2008	43° 59.92' S, 146° 19.31' E	227

Electronic annex 2. Mercury species distribution in the coastal sea ice environment 12 km northeast of the Casey Station (Australian East Antarctic sector) (66° 13'S; 110° 39'E).

Date	Medium	Depth	Salinity	Chl*a*	POC	Hg_T	Hg_R	$MeHg_T$	$MeHg_T/Hg_T$
		cm		*µg.L^{-1}*	*µg.L^{-1}*	*pmol L^{-1}*	*pmol L^{-1}*	*pmol L^{-1}*	*%*
11/11/09	Sea ice	0-6	-	0.07	252	22.33	17.9	0.145	0.6
11/11/09	Sea ice	30-36	5.9	0.06	614	7.17	0.68	0.36	5
11/11/09	Sea ice	70-76	4.9	0.52	226	3.54	0.78	0.321	9.1
11/11/09	Sea ice	108-114	5.9	4.48	860	3.31	0.45	0.267	8.1
11/11/09	Sea ice	114-120	11.2	91.3	11196	8.92	0.95	-	-
14/11/09	Sea ice	0-6	1.7	0.1	288	28.42	10.39	0.082	0.3
14/11/09	Sea ice	30-36	4.6	0.04	226	3.61	1.67	<0.045	<1.3
14/11/09	Sea ice	70-76	4.4	0.36	205	0.9	0.27	<0.045	<5.0
14/11/09	Sea ice	106-112	6.1	3.44	750	5.12	0.28	<0.045	<0.9
14/11/09	Sea ice	112-118	12.1	247.62	25176	6.47	0.46	0.281	4.3
14/11/09	Sack-hole brine	50	54.5	0.05	749	12.69	11.15	0.083	0.7
14/11/09	Sack-hole brine	100	65.3	0.24	543	15.24	15.15	0.158	1
14/11/09	Seawater	0	33.7	0.68	95	44.4	25.89	0.155	0.3
14/11/09	Seawater	500	34.3	0.03	32	27.85	18.83	0.142	0.5
14/11/09	Seawater	1000	33.6	0.06	23	6.31	-	0.155	2.5
17/11/09	Snow	-	-	-	-	27.78	19.6	0.344	1.2
17/11/09	Sea ice	0-6	5.5	0.32	289	-	10.63	0.129	-
17/11/09	Sea ice	30-36	4.8	0.08	226	3.43	2.23	0.241	7
17/11/09	Sea ice	70-76	4	0.22	205	6.51	2.41	0.247	3.8
17/11/09	Sea ice	106-112	6.4	4.21	750	4.71	3.53	0.277	5.9
17/11/09	Sea ice	112-118	11.2	81.2	25176	4.48	1.96	0.44	9.8
17/11/09	Sack-hole brine	50	57.1	0.22	748	14.67	6.84	0.115	0.8
17/11/09	Sack-hole brine	100	52.4	0.14	543	13.29	3.37	0.029	0.2
17/11/09	Seawater	0	33.9	0.04	95	17.24	9.94	0.284	1.6
17/11/09	Seawater	500	35.4	0.05	32	11.71	6.01	0.234	2
17/11/09	Seawater	1000	33.7	0.04	23	18.89	11.9	0.269	1.4

20/11/09	Sea ice	0-6	1.9	0	153	-	-	-	-
20/11/09	Sea ice	30-36	5.2	0.21	476	-	-	-	-
20/11/09	Sea ice	70-76	3.6	0.08	315	-	-	-	-
20/11/09	Sea ice	106-112	6.6	2.17	951	-	-	-	-
20/11/09	Sea ice	112-118	12.3	126.8	15418	-	-	-	-
20/11/09	Sack-hole brine	50	46.9	0.22	588	24	23.16	<0.045	<0.2
20/11/09	Sack-hole brine	100	39.6	0.21	407	8.85	8.83	0.206	2.3
20/11/09	Seawater	0	33.7	0.55	53	1.72	1.36	0.066	3.8
20/11/09	Seawater	500	33.6	0.04	55	1.58	1.2	0.084	5.3
20/11/09	Seawater	1000	33.3	0.01	36	1.21	1.15	0.078	6.5

Electronic annex 3. Principal Component Analysis on salinity, particulate organic carbon (POC), chlorophyll *a* (Chl*a*), total mercury (Hg_T), reactive mercury (Hg_R) and total methylated mercury ($MeHg_T$) within the snow, ice, brine and seawater in the coastal sea ice environment 12 km northeast of the Casey Station (Australian East Antarctic sector) (66° 13'S; 110° 39'E).

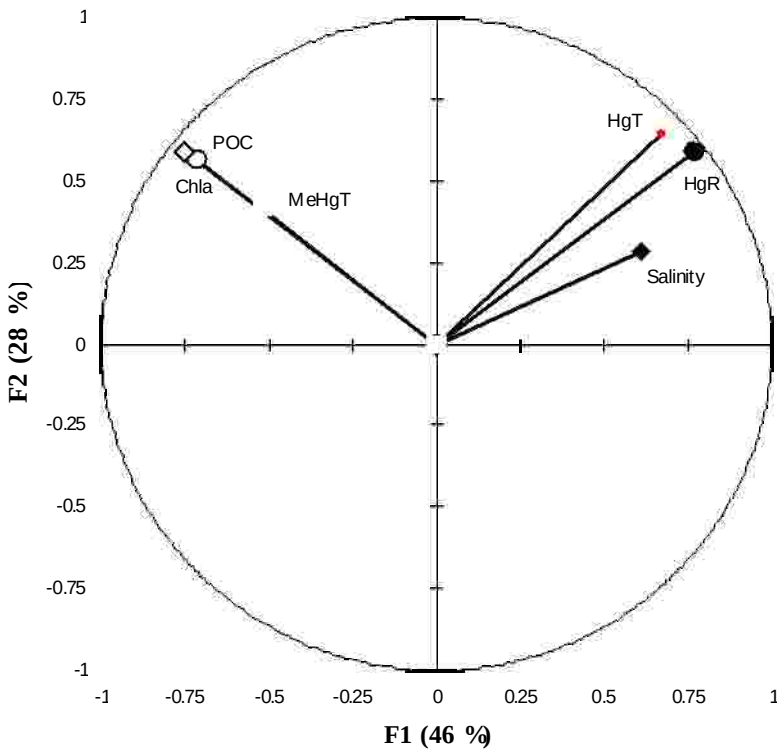

Electronic annex 4. SR3 CASO-GEOTRACES transect. Vertical distribution of total methylated m ury ($MeHg_T$) against potential density evidencing latitudinal gradient along isopycnals.

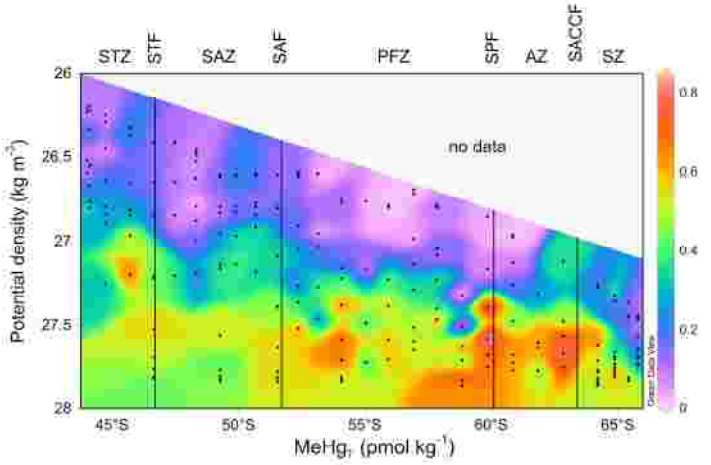

Electronic annex 5. SR3 CASO-GEOTRACES transect. Vertical distribution of apparent oxygen utilization (AOU) distributions against potential density evidenci titudinal gradient along isopycnals

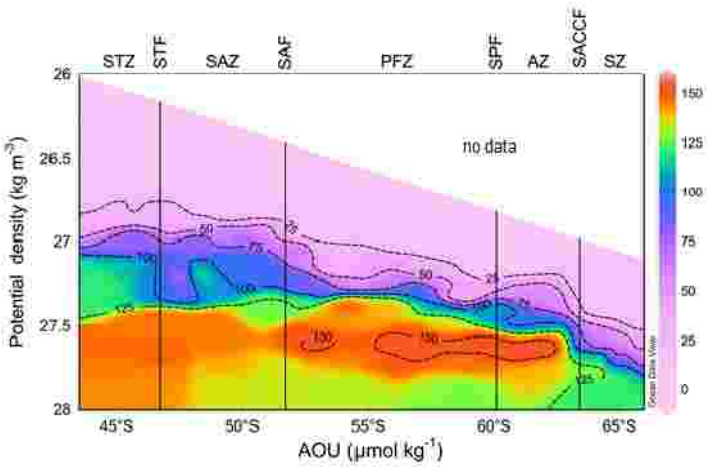

Electronic annex 6. Correlations between $MeHg_T$ concentrations and AOU within the first 1000 m of the water column of the Southern Ocean (SR3 CASO-GEOTRACES section). STZ: Subtropical Zone; SAZ: Subantarctic Zone; PFZ: Polar Frontal Zone; AZ: Antarctic Zone; SZ: Southern Zone.

Zone	Station	Regression coefficient ($pmol_{MeHgT}$ / μmol_{AOU})	R^2	Significance (p)
SZ	1	0.0031	0.939	< 0.01
SZ	2	0.0040	0.876	< 0.01
SZ	3	0.0050	0.976	< 0.01
AZ	4	0.0028	0.467	> 0.10
AZ	5	0.0028	0.751	< 0.10
AZ	6	0.0033	0.894	< 0.01
AZ	7	0.0042	0.979	< 0.01
AZ	8	0.0051	0.941	< 0.01
PFZ	9	0.0019	0.217	> 0.10
PFZ	10	0.0034	0.885	< 0.01
PFZ	11	0.0033	0.990	< 0.01
PFZ	12	0.0037	0.953	< 0.01
PFZ	13	0.0027	0.966	< 0.01
PFZ	14	0.0039	0.930	< 0.01
PFZ	15	0.0023	0.716	< 0.10
SAZ	16	0.0023	0.802	< 0.10
SAZ	17	0.0023	0.982	< 0.01
SAZ	18	0.0023	0.544	> 0.10
SAZ	19	0.0016	0.593	> 0.10
SAZ	20	0.0016	0.791	< 0.10
SAZ	21	0.0012	0.599	> 0.10
SAZ	22	0.0028	0.611	< 0.10
STZ	23	0.0024	0.941	< 0.01
STZ	24	0.0039	0.915	< 0.01
STZ	25	0.0020	0.597	< 0.10
STZ	26	0.0050	0.430	> 0.10
STZ	27	0.0002	0.163	> 0.10